Microchemical Journal 194 (2023) 109326

Contents lists available at ScienceDirect

Microchemical Journal

journal homepage: www.elsevier.com/locate/microc

Outstanding glucose sensing properties of N-doped carbon nanotubes boosted by Co(II) and Cu(II) ions in alkaline electrolytes

Zanling Huang [a], Shuqi Zhu [a], Abebe Reda Woldu [a], Wenhua Gao [a], Jing-Xin Jian [a], Paul K. Chu [c], Qing-Xiao Tong [a,*], Liangsheng Hu [a,b,*]

[a] Department of Chemistry and Key Laboratory for Preparation and Application of Ordered Structural Materials of Guangdong Province, Shantou University, Shantou 515063, PR China
[b] Chemistry and Chemical Engineering Guangdong Laboratory, Shantou 515063, PR China
[c] Department of Physics, Department of Materials Science and Engineering, and Department of Biomedical Engineering, City University of Hong Kong, Tat Chee Avenue, Kowloon, Hong Kong, China

ARTICLE INFO

Keywords:
Glucose detection
Cobalt
Copper
Carbon nanotubes

ABSTRACT

Electrochemical glucose detection co-catalyzed by bimetallic ions is carried out by introducing Co(II) and Cu(II) into the alkaline solution. The technique avoids the complicated electrode design and catalyst poisoning. By using nitrogen-doped carbon nanotubes (NCNT) loaded on carbon cloth (CC) as the working electrode, the bimetal co-catalytic system achieves a sensitivity of 6,909 mA M^{-1} cm^{-2}, a detection limit of 0.4 μM (S/N = 3), as well as good selectivity and stability. By performing systematic electrochemical and structural analysis, the mechanism of Co(II) and Cu(II) co-catalysis for glucose detection in the solution is elucidated. Co(II) supplies the dynamic reaction sites and source of active intermediate (CoOOH), while Cu(II) promotes the formation of CoOOH. The results provide mechanistic insights into bimetal co-catalysis of glucose detection and other electrochemical reactions.

1. Introduction

As one of the common organic substances, glucose is an important energy source in the human body and vital to the normal functioning of organs [1–3]. Diabetes is a metabolic disorder arising from an excess amount of glucose in the blood and can cause a series of complications such as hypertension, renal dysfunction, and strokes [4]. Diabetes has become an increasingly prevalent global disease, especially in middle- and low-income countries [5,6]. Without a complete cure, glucose monitoring is necessary for the diagnosis and treatment of diabetes [7,8] and the demand for a cheap, fast, and reliable method to detect glucose is high.

Among the techniques for glucose monitoring such as fluorescence, photoacoustic resonance, Raman spectroscopy, and metal oxide-based field effect transistors, electrochemical detection based on non-enzymatic method is especially attractive because of the high sensitivity, low detection limit, fast response, convenience, low cost, and being suitable for real-time detection [9–16]. Recently, non-enzymatic glucose sensors composed of nanomaterials have attracted enormous research interest [17]. In the sensors, the electrocatalysts on the electrode react with glucose to generate an electrical signal and the efficiency and accuracy depend on the properties of the sensing nanomaterials [18]. At present, different nanomaterials have been proposed for glucose electrooxidation, including noble metals (Au [19], Pd [20], Pt [21], etc.), non-noble metals (Co [22], Cu [23], Ni [24], etc.), carbon-based materials [25], and conductive polymers [26]. Owing to the lower cost compared to noble metals, relatively high electrocatalytic activity, and chemical stability, transition metals such as Co, Cu, and Ni, their oxides/hydroxides, and chalcogenides have gathered substantial interest [27–30].

The detection mechanism is based on the interactions between the multivalent metal species and glucose. In general, multivalent metal species are generated *in situ* on the electrocatalysts in an alkaline electrolyte to provide the oxidants for glucose electrooxidation. Specifically, after electrooxidation of M^{n+} to M^{n+1} (M = Cu, Co, and Ni), the glucose molecules reduce the strongly oxidizing M^{n+1} species to regenerate M^{n+} [31]. To achieve satisfactory glucose detection, efforts have been made to increase the number of active sites on the electrocatalysts to reach

* Corresponding authors at: Department of Chemistry and Key Laboratory for Preparation and Application of Ordered Structural Materials of Guangdong Province, Shantou University, Shantou 515063, PR China (L. Hu).
E-mail addresses: qxtong@stu.edu.cn (Q.-X. Tong), lshu@stu.edu.cn (L. Hu).

https://doi.org/10.1016/j.microc.2023.109326
Received 24 July 2023; Received in revised form 3 September 2023; Accepted 5 September 2023
Available online 7 September 2023

high activity and sensitivity in glucose electrooxidation. Combining various metals and/or metallic compounds is one of the effective strategies to alter the electronic structure and increase the active sites of nanomaterials. Multi-metallic catalysts deliver better electrocatalytic performance than single-component electrodes due to their synergistic activity and more active sites [26,32]. It has been reported that transition metals in the composites change from a low valence state to high valence state in the form of metal oxyhydroxide. Two or more than two metal oxyhydroxides rapidly oxidize glucose into gluconolactone in conjunction with simultaneous chemical reduction. However, there is no consensus on which metal plays the main role. Bimetallic structures comprising different metals and different combinations have been explored, for instance, CuCo [4,33,34], NiCo [35,36], CuNi [37], and NiFe [38] to exploit the synergistic effects. Yuan et al. [33] designed and synthesized the nanowire-constructed coral-like Cu-Co-mixed oxides (Cu-Co-O) on Ni foam by combining a hydrothermal method and thermal annealing process. The unique nanoarchitecture with abundant electro-active sites and ions-transfer channels, as well as the synergistic effect of copper and cobalt ions in the spinel crystal, endowed the Cu-Co-O modified electrode with prominent electrocatalytic performance toward the oxidation of glucose. Although the sensitivity has been improved, problems such as the long-term stability and surface poisoning have not been solved. Moreover, the use of sophisticated nanostructures inevitably raises the fabrication cost, thereby contradicting the original intention of designing a cheap glucose sensing system. Meanwhile, the approaches to synthesize nanomaterials, such as hydrothermal treatment, thermal annealing, electro-deposition, and micro-plasma are usually clumsy and time-consuming as well as sophisticated equipment involved [39,40].

Based on the concept of maximization of active sites, we have previously described a simple and efficient strategy for glucose electrooxidation by using M^{n+} (Cu(II), Co(II), Ni(II)) ions in an alkaline electrolyte [5,41,42]. Different from the solid electrocatalysts, the homogeneously dispersed ions are engaged as the electrocatalysts to allow interactions between the metal sites and glucose. The M^{n}-glucose complex serves as the reactant near the electrode surface and is oxidized to the M^{n+1}-glucose intermediates which eventually produce gluconate ions to regenerate the M^{n} species. The high efficiency of the M^{n+}-mediated catalytic system gives rise to excellent electrochemical glucose sensing properties. Since every M atom is engaged as an active catalytic site, the maximum atomic efficiency and better sensitivity are accomplished. As mixed transition-metal composites have demonstrated higher electrochemical activity in glucose electrooxidation than the single-counterpart metal due to the synergistic effects offered by two metals, including the complex chemical composition and structure as well as redox ability [4,33,43], the performance of double transition-metal ions co-catalysis is of particular interest.

Inspired by the ion-catalytic effect and synergetic activity of multi-metal composites, glucose electrooxidation co-catalyzed by homogenously dispersing Co(II) and Cu(II) in the alkaline electrolyte is investigated in this work. The novel design of this system is different from the current strategies that usually employ solid–liquid interfaces on electrode to realize glucose detection, which is time- and energy-saving and avoids complicated catalyst/electrode design and catalyst poisoning. The electrochemical properties of metal ions towards glucose detection are studied by cyclic voltammetry (CV) and amperometric (*i*-t) measurements with nitrogen-doped carbon nanotubes coated on carbon cloth (NCNT/CC) as the electrode. By comparing the electrochemical results of NCNT/CC catalyzed by the single metal ion (Co(II) or Cu(II)) as well as two metallic ions (Co(II)&Cu(II)) with different addition sequence, it is observed that the bimetal systems deliver better performance than the single counterpart. The bimetal-ion catalytic systems (Co(II)&Cu(II)) with the one Co(II) added first has better properties. Based on systematic characterization by SEM, TEM, and XPS, CoOOH is proposed to be main active intermediate and addition of Cu(II) promotes the generation of the intermediate to improve the glucose oxidation characteristics. The kinetics is assessed by CV conducted at different scanning rates, C_{dl}, and EIS. The electrode co-catalyzed by Co(II)&Cu(II) has excellent glucose sensing properties including a high sensitivity of 6,909 mA M^{-1} cm^{-2}, low limit of detection (LOD) of 0.4 μM, as well as good selectivity and stability.

2. Experimental section

2.1. Chemicals

Cobalt (II) nitrate (99.99%), Copper (II) nitrate (99%), Iron (III) nitrate (99%), L-ascorbic acid (98%) were purchased from Saen Chemical Technology. Nickle (II) nitrate (AR), sodium hydroxide (AR), α-lactose (AR), L-phenylalanine (AR), ethanol (AR), D-(+)-glucose (AR), and dopamine (AR) were purchased from Aladdin. Glycine (AR) and sodium chloride (AR) was obtained from Xilong Scientific Co., Ltd. and Sinopharm Group Chemical Reagent Co., Ltd., respectively. NCNTs (0D: 30–80 nm, L:10–30 μM) and carbon cloth (CC) were obtained from SaiBo Electrochemical Materials Network and Nafion (5 wt%) was purchased from Tianjin IncoleUnion Technology. All the chemicals were used as received and the aqueous solution was prepared using ultrapure water (18.2 MΩ cm^{-1}).

2.2. Characterization

Scanning electron microscopy (SEM) and energy dispersive X-ray spectroscopy (EDS) were conducted on a field-emission scanning electron microscopy (Gemini 300) equipped with EDS. Transmission electron microscopy (TEM) was performed on the FEI Titan G2 60–300. The X-ray diffraction (XRD) patterns were collected on the Mini Flex 600 powder X-ray diffractometer and X-ray photoelectron spectroscopy (XPS) was carried on the Thermo Fisher Nexsa instrument.

2.3. Sample preparation

The CC was sonicated successively in acetone, ethanol, and distilled water for 15 min each and then dried at 60 ℃ in an oven. After drying, CC was cut into an area of 0.5 × 0.5 cm^2 for the working electrode support. To prepare the modified NCNT/CC and CNT/CC, 5 mg of NCNT or CNT were dispersed in a solution containing 750 μL of ethanol, 250 μL of DI water, and 20 μL of Nafion (5 wt%). Then 10 μL of NCNT or CNT ink was dropping cast on CC (5 μL for each side). The electrodes were dried at room temperature for 3 h before the test with CNT used for comparison. The N atom sites in NCNT serve as additional occupied sites for Co(II) and Cu(II) ions [44].

2.4. Electrochemical measurements

A three-electrode system was used in the electrochemical measurements with NCNT/CC and CNT/CC as the working electrodes. The saturated calomel electrode (SCE) and platinum wire were the reference and counter electrodes, respectively. The electrochemical measurements were performed on the CHI 660E electrochemical workstation. In the experiments, 1.0 M NaOH (pH = 13.7) is the electrolyte. Cyclic voltammetry (CV) and amperometric (*i*-t) measurements were performed to evaluate the glucose electrooxidation characteristic of NCNT/CC and CNT/CC co-catalyzed by Co(II)&Cu(II). The CV scanning rate was 10 mV s^{-1}. In the *i*-t tests, after applying a target potential, various amounts of the $Co(NO_3)_2$ and $Cu(NO_3)_2$ solutions (0.1 M) were added to the electrolyte at 100 s and 550 s, respectively. When the background current stabilized, the glucose solution was added every 50 s under stirring at 1,050 rpm. Electrochemical impedance spectroscopy (EIS) was conducted from 10 mHz to 1 MHz at 0.51 V (vs. SCE, the same below if not specifically stated). The double layer capacitance (C_{dl}) was obtained from the CV curves in the non-Faradaic potential window (0.2–0.3 V) at different scanning rates of 100, 120, 140, 160, 180, and 200 mV s^{-1}. At

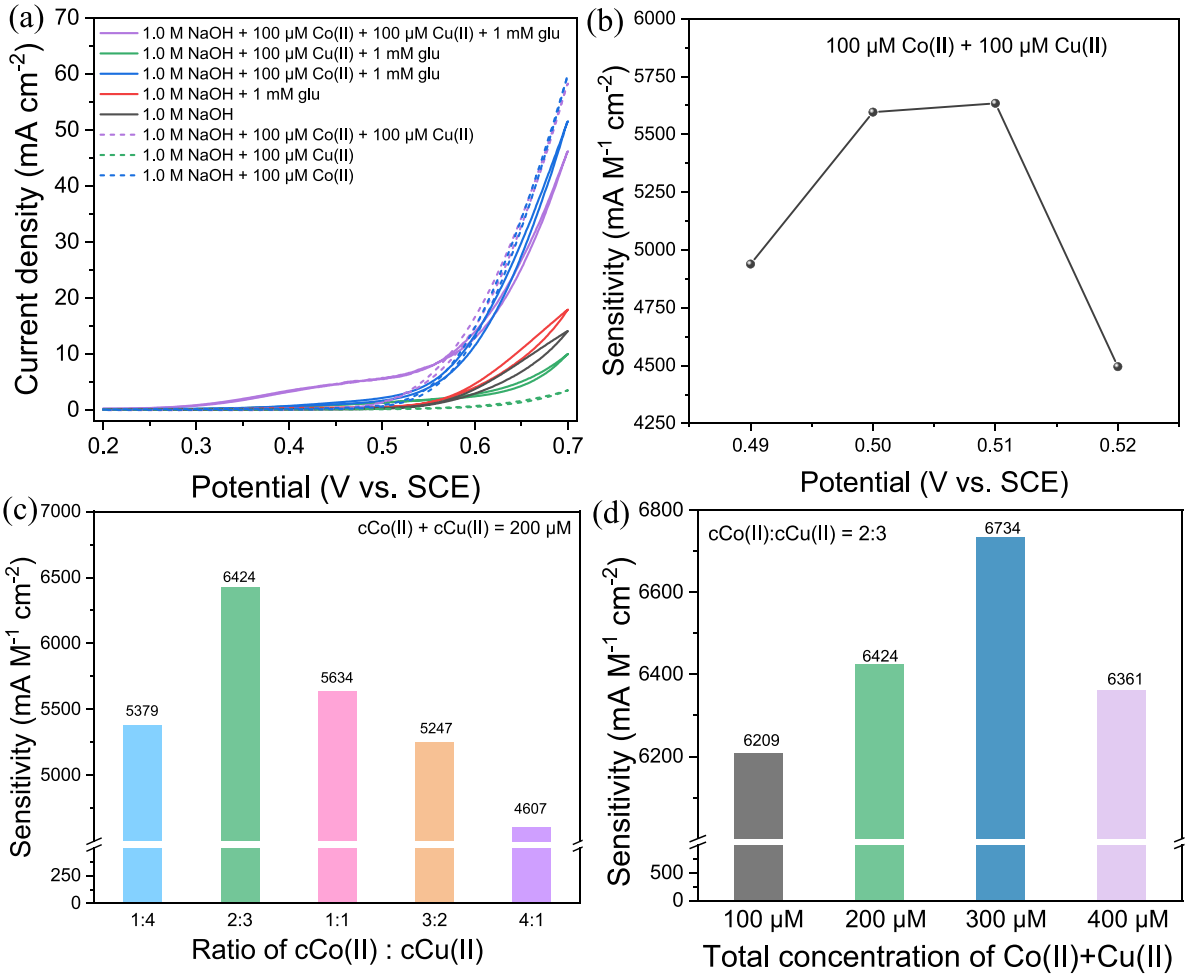

Fig. 1. (a) CVs of NCNT/CC in NaOH, NaOH + Co(II) and/or Cu(II), NaOH + glucose (glu), NaOH + Co(II) and/or Cu(II) + glu; Sensitivity of NCNT/CC with (b) Co (II) + Cu(II) at different applied potentials, (c) different ion concentration ratios of c(Co(II)):c(Cu(II)), and (d) different total ion concentrations.

0.25 V (the middle of the cycle curve), half of the difference in the current density ($1/2(j_{anodic}-j_{cathodic})$) was represented as the value of the y-coordinate. C_{dl} was estimated by plotting the difference of the current density against scanning rates. That is, the ordinate is the difference in the current density, and the abscissa is the scanning rate.

3. Results and discussion

3.1. Proof-of-concept experiment with Co(II) as the electrocatalyst

Co(II) has high catalytic effects in glucose electrooxidation in the alkaline electrolyte involving successive electrooxidation of Co(II)- to Co (III)- and Co(IV)-glucose and then dissociation of Co(IV)-gluconolactone complex to regenerate Co(III) species in the double layer region to form the Co(III)-glucose intermediate in a new cycle [41]. In the proof-of-concept experiment, the electrochemical characteristics of the soluble Co(II) species were studied by the CVs on NCNT/CC electrode. CV was conducted in 1.0 M NaOH solution containing 1 mM glucose and different concentrations of Co(II) (0, 10, 50, 100, 200, and 400 μM). Fig. S1a compares the CVs of glucose with different concentrations of Co (II). In the absence of Co(II), the response current of glucose is small in the potential range of 0.2–0.7 V. This small current is attributed to the competition between glucose electrooxidation and the oxygen evolution reaction (OER). Upon addition of Co(II), the current density increases with increasing concentrations of Co(II) between 0.4 and 0.7 V, proving that Co(II) is the electrocatalyst for glucose electrooxidation. The sensitivity obtained from *i*-t curves indicates that 100 μM is the optimal concentration of Co(II) for glucose electrooxidation (Fig. S1b).

3.2. Co-catalysis of glucose electrooxidation by Co(II)&Cu(II) ions

It has been reported that bimetallic catalysts possess more optimized chemical structures and variable oxidation valences for better glucose sensing than the mono-metallic counterparts [4,22,33,35,43]. Hence, it is anticipated that introducing bimetal ions into the electrolyte will lead to better performance and the effects are investigated by performing CV in the presence of different bimetal ions. The CVs were acquired from 1.0 M NaOH containing 1 mM glucose and ions such as Cu(II) and Co(II) (Fig. S2a), Ni(II) and Co(II) (Fig. S2b), Fe(III) and Co(II) (Fig. S2c), Cu(II) and Ni(II) (Fig. S2d), Cu(II) and Fe(III) (Fig. S2e), as well as Ni(II) and Fe (III) (Fig. S2f). Considering that there is competition between glucose electrooxidation and OER in the alkaline electrolyte, the effects can be revealed from the current density enhancement after addition of ions. As shown in Fig. S1a, higher current densities between 0.4 and 0.7 V are observed after adding Co(II) indicating that Co(II) is the catalyst for glucose electrooxidation. The glucose molecules occupy the coordination sites of Co(II) thus preventing the essential Co(II)–OH-coordination for OER. As shown in Fig. S2a, addition of Cu(II) increases the current densities between 0.4 and 0.56 V, while the current densities between 0.56 V and 0.7 V decrease, suggesting that Cu(II) boosts glucose electrooxidation and impedes OER. As shown in Fig. S2b, the CVs acquired after adding Ni(II) ion show almost no change and therefore, Ni(II) is not the catalyst for glucose electrooxidation or OER. The enhanced current densities upon incorporation of Fe(III) between 0.5 and 0.7 V indicate

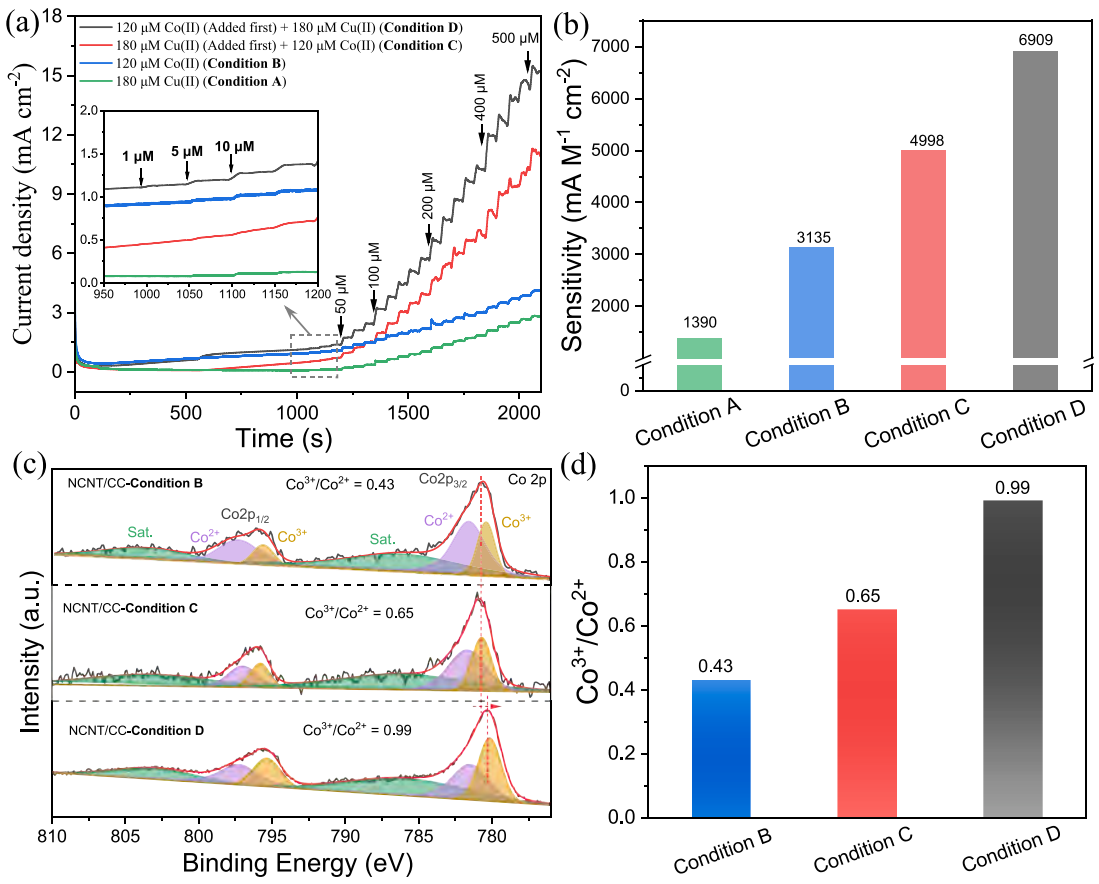

Fig. 2. (a) *i*-t curves of the NCNT/CC electrodes for glucose detection catalyzed by Cu (Condition A), Co (Condition B), Cu(II)&Co (Condition C), and Co&Cu(II) (Condition D) and (b) Corresponding sensitivity; (c) Co 2*p* spectra and (d) Co^{3+}/Co^{2+} ratios of NCNT/CC after glucose detection catalyzed by Co (Condition B), Cu (II)&Co (Condition C), and Co&Cu(II) (Condition D).

that Fe(III) ions catalyze OER but not glucose electrooxidation. It can be inferred that both Co(II) and Cu(II) enhance oxidation of glucose, while Fe(III) mainly enhances water oxidation. Furthermore, by comparing the current density increase between 0.4 and 0.7 V, Co(II) and Cu(II) are considered the best bimetal ion combination for glucose electrooxidation. Fig. 1a displays the CVs of NCNT/CC in 1.0 M NaOH, 1.0 M NaOH with 100 μM Co(II) and 100 μM Cu(II) alone and together, 1.0 M NaOH with 1 mM glucose, 1.0 M NaOH in presence of 1 mM glucose with 100 μM Co(II) and 100 μM Cu(II) alone or together. It is evident that both Co(II) and Cu(II) alone can enhance glucose electrooxidation, while the combination of them have synergistic effects leading to higher current increase in glucose detection.

3.3. *Optimal conditions for glucose electrooxidation co-catalyzed by Co (II)&Cu(II)*

We first optimize the reaction potential for glucose electrooxidation with 100 μM Co(II) and 100 μM Cu(II). Fig. S3a shows the amperometric response of NCNT/CC to different concentrations of glucose (10, 20, 200, and 1000 μM, respectively) in 1.0 M NaOH containing 100 μM Co (II)&100 μM Cu(II) at different applied potentials (0.49, 0.50, 0.51, and 0.52 V). The current density increment caused by a certain concentration of glucose under given conditions (100 μM Co(II) + 100 μM Cu(II) and applied potential) is used to evaluate the catalytic activity. A high sensitivity indicates high activity towards glucose electrooxidation. The sensitivities under the conditions of 0.49, 0.50, 0.51, and 0.52 V are calculated to be 4,939, 5,596, 5,634, and 4,495 mA M^{-1} cm^{-2} in the range of 10 μM-0.56 mM, respectively, indicating that 0.51 V is the optimal potential (Fig. 1b). The small potentials provide a poor glucose electrooxidation ability, while at a higher potential, both OER and glucose electrooxidation are competing for the limited M(II) sites consequently limiting the reaction rate of glucose electrooxidation.

We then determine the optimal concentration ratio of Co(II):Cu(II) for a total metal ion concentration of 200 μM by applying a glucose oxidation potential of 0.51 V. The CVs in Fig. S4a are used to determine the different response to glucose electrooxidation of NCNT/CC in NaOH + glucose without or with different concentration ratios (1:4, 2:3, 1:1, 3:2, and 4:1) of Co(II):Cu(II). At 0.51 V, the current response co-catalyzed by Co(II):Cu(II) has ratios of 1:4, 2:3, 1:1, and 3:2 and is nearly the same, whereas the ratio of 4:1 exhibits less enhancement than the other ratios. The corresponding sensitivities are calculated to be 5,379, 6,424, 5,634, 5,247, and 4,607 mA M^{-1} cm^{-2} in the range of 10 μM-0.56 mM, respectively, indicating that a cCo(II):cCu(II) ratio of 2:3 is optimal (Fig. 1c).

The total concentration of metal ions determines the number of active sites for glucose coordination and electrooxidation. Therefore, the correlation between the total concentration of Co(II)&Cu(II) and glucose electrooxidation activity is studied and the amperometric responses are shown in Fig. S5a. The sensitivity exhibits a volcano shape and the highest sensitivity is obtained at the medium total concentration of 300 μM (Fig. 1d). At low total concentrations, adding additional metal ions can provide more active sites for glucose coordination and electrooxidation to enhance the activity. However, too many metal ions result in a higher kinetic barrier for mass transfer to the surface of the NCNT/CC electrode. Fig. 1d discloses that the highest sensitivity of 6,734 mA M^{-1} cm^{-2} is achieved by 120 μM Co(II) + 180 μM Cu(II).

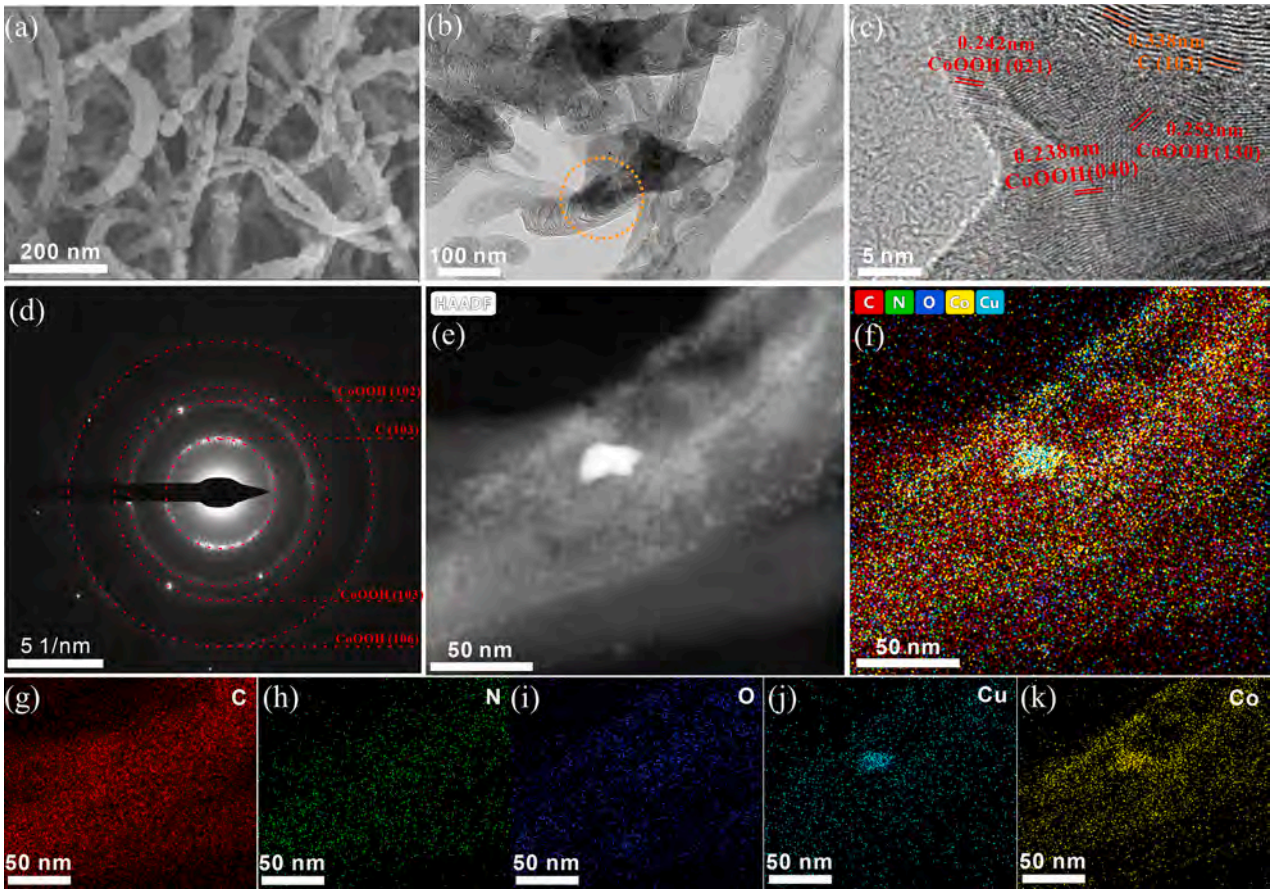

Fig. 3. (a) SEM image, (b, c) TEM images, (d) SAED pattern, (e) HAADF image, and (f-k) EDS maps of NCNT/CC after glucose determination catalyzed by Co&Cu (Condition D).

3.4. Roles of Co(II) and Cu(II) ions

To determine the roles of Co(II) and Cu(II) ions in the catalytic system, the *i*-t curves of NCNT/CC electrode for glucose detection are compared with those of different ion combinations including 180 μM Cu (II) (Cu, Condition A), 120 μM Co(II) (Co, Condition B), 180 μM Cu(II) (first added) + 120 μM Co(II) (Cu&Co, Condition C), 120 μM Co(II) (first added) + 180 μM Cu(II) (Co&Cu, Condition D), respectively. As shown in Fig. 2a, the electrodes catalyzed by bimetal-ions show higher currents after glucose addition than single metal-ion, while Co(II) has a more obvious catalytic effect. It is surprising that with different ion addition sequences, the glucose electrooxidation performance also differs. Adding Co(II) first and then Cu(II) produces better characteristics. The sensitivities calculated from Fig. 2a are 6,909, 4,998, 3,135, and 1,390 mA M^{-1} cm^{-2} in the range of 0.4 μM-0.56 mM, respectively (Fig. 2b).

The morphologies of the NCNT/CC working electrodes before and after glucose electrooxidation are examined by SEM as shown in Fig. S6a and S6f. The blank NCNT/CC are nanotubes with a smooth surface. After glucose detection, a thick layer with particles wraps around the nanotubes. To analyze the thick layer, another NCNT/CC electrode is tested in 1.0 M NaOH with Co(II)&Cu(II) for the same time of 2,200 s except without glucose addition. The morphology (Fig. S6e) is similar to that tested in the solution containing glucose, indicating that the thick layer is the intermediate product of Cu(II) or Co(II) oxidation, but not the glucose oxidation. The other control samples including those tested in Co(II)&Cu(II), Co(II) only, and Cu(II) only solutions for 1000 s (before glucose is introduced in the amperometric test) shown in Fig. S6b-S6d confirm that the thick layer may be the oxidation intermediate of Co(II) as almost no changes are observed compared to the bare NCNT/CC and the electrode with only Cu(II) addition. it is speculated that Co(II) acts as the dynamic reaction sites and the source of active intermediates (CoOOH), while Cu(II) promotes the formation of CoOOH. The EDS maps of NCNT/CC after glucose detection reveal uniform distributions of C, N, O, Co, and Cu (Fig. S7). However, all the samples have similar diffraction patterns just showing the peaks indexed to carbon without evident difference in the XRD patterns (Fig. S8), this may be due to that the oxidation intermediate is amorphous or the content is too low to be detected by XRD. Fig. S9 shows the XPS survey spectra of blank NCNT/CC and the one after glucose detection catalyzed by Co (Condition B), Cu&Co (Condition C), and Co&Cu (Condition D). All the samples exhibit the peaks of O 1 *s*, N 1 *s*, and C 1 *s*. In addition, the Co 2*p* peaks emerge from the NCNT/CC catalyzed by Co (Condition B), Cu&Co (Condition C), and Co&Cu (Condition D), while the Cu 2*p* peaks only appear from the samples catalyzed by Cu&Co (Condition C) and Co&Cu (Condition D). Fig. 2c shows the Co 2*p* spectra of NCNT/CC after glucose addition. The peaks at 786.0 and 803.6 eV are assigned to the Co $2p_{3/2}$ and Co $2p_{1/2}$ spin-orbitals, respectively. The peaks at 780.4 and 795.6 eV can be indexed to Co^{3+}, and those at 781.6 and 797.3 eV correspond to Co^{2+} [15]. Compared to the NCNT/CC catalyzed by Co (Condition B), the samples catalyzed by Cu&Co (Condition C) and Co&Cu (Condition D) have larger concentrations of Co^{3+}. The sample of condition D has a larger percentage of Co^{3+} than that of condition C (Fig. 2d). The larger concentration of Co^{3+} of NCNT/CC (Condition D) compared to that of condition B indicates the formation of high valence Co^{3+} when adding Co(II) ions to the alkaline solution and that Cu incorporation promotes the generation of more CoOOH to improve glucose electrooxidation [45,46]. The binding energy shift of the Co $2p_{3/2}$ peak is associated with Cu induced electron transfer. The Cu 2*p* spectra of the sample (Fig. S10a) after glucose detection show two peaks at 933.8 and 942.8 eV attributed to Cu(II) species and the well-known shake-up satellite peak [44]. The O

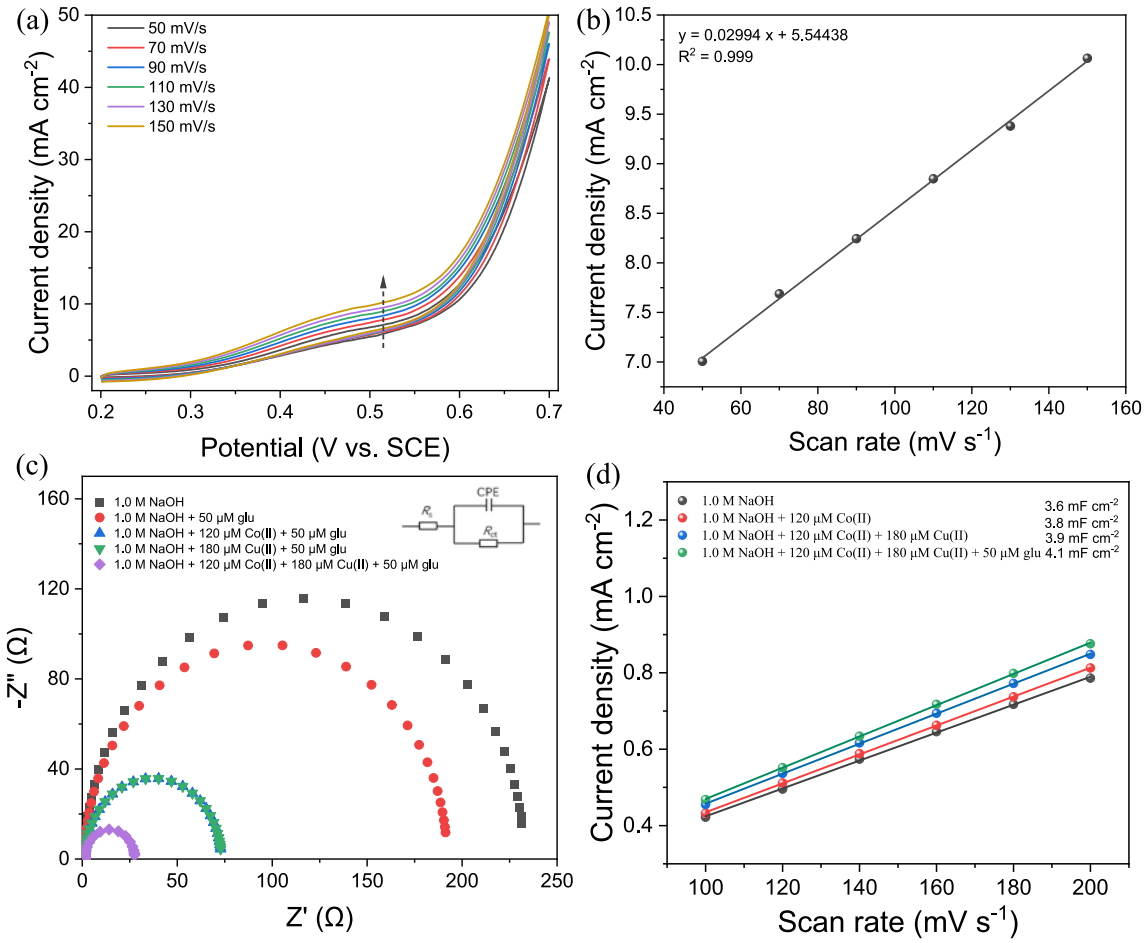

Fig. 4. (a) CVs of NCNT/CC acquired at different scanning rates in presence of Co&Cu and 1 mM glucose in 1.0 M NaOH aqueous solution and (b) Corresponding linear relationship; (c) EIS plots and (d) C_{dl} values of NCNT/CC in 1.0 M NaOH, 1.0 M NaOH with 50 μM glucose, 1.0 M NaOH with 50 μM glucose and Co, 1.0 M NaOH with 50 μM glucose and Cu, and 1.0 M NaOH with 50 μM glucose and Co&Cu.

1 *s* spectra of NCNT/CC (Fig. S10b) can be deconvoluted into those of absorbed oxygen (532.4 eV) and C-O (535.5 eV) [5,15]. After glucose detection, the peak of C-O disappears, while absorbed oxygen increases and shifts to a smaller binding energy due to the interactions between oxygen and Co(II)&Cu(II). The N 1 *s* spectra (Fig. S10c) indicate that the electrodes are almost unchanged before and after glucose detection.

To further understand the process and mechanism of glucose sensing, the morphology, crystalline phase, and elemental distribution of the electrodes after glucose electrooxidation catalyzed by Co&Cu (Condition D) are investigated by SEM and TEM. As shown in Fig. 3a (SEM) and Fig. 3b (TEM), the smooth NCNTs (Fig. S6a) are coated with nanoparticles after electrochemical glucose determination catalyzed by Co&Cu, indicating creation of important intermediates during the process. Fig. 3c presents the HR-TEM image of the enlarged view of the orange circle in Fig. 3b. The d-spacing of 0.338 nm is assigned to the C (1 0 3) plane and the interplanar spacings of 0.232, 0.238, 0.242, and 0.253 nm are associated with the (1 1 1), (0 4 0), (0 2 1), and (1 3 0) planes of CoOOH, respectively, demonstrating that the *in situ* generated intermediate during glucose detection is CoOOH. This is confirmed by the selected-area electron diffraction (SAED) patterns (Fig. 3d) showing the C and CoOOH phases. No Cu-based materials are found by TEM. However, the high-angle annular dark-field scanning TEM (HAADF-STEM) image (Fig. 3e) and the EDS maps (Fig. 3f-k) reveal uniform distributions of C, N, O, Cu, and Co. Therefore, considering the SEM, XPS, TEM, and EDS results, Cu is incorporated into the CoOOH intermediate during the electrochemical process.

3.5. Kinetics of glucose electrooxidation co-catalyzed by Co(II)&Cu(II) ions

To understand the kinetics of glucose electrooxidation catalyzed by Co&Cu (Condition D), CVs at different scanning rates, EIS, and C_{dl} are measured. Fig. 4a shows the effects of different scanning rates on oxidation of glucose on the NCNT/CC electrode co-catalyzed by Co(II) and Cu(II) ions with scanning rates from 50 to 150 mV s^{-1}. The oxidation current increases with scanning rates, which is consistent with the linear fitting of the relationship between the reaction current and scanning rates in Fig. 4b, showing that the oxidation current at 0.51 V has an excellent linear relationship with the scanning rate with a correlation coefficient of 0.999. These results indicate that the electrochemical kinetics of NCNT/CC co-catalyzed by Co(II) and Cu(II) ions is mainly adsorption control on the electrode surface [15].

EIS is employed to investigate the kinetics of glucose electrooxidation by Co(II)&Cu(II) co-catalysis. The frequency response of NCNT/CC is monitored in 1.0 M NaOH containing Co(II) and/or Cu(II) with 50 μM glucose in the frequency range between 10 mHz and 1 MHz at a bias potential of 0.51 V at which glucose electrooxidation takes place. Fig. 4c shows the Nyquist plots of the Co(II) and/or Cu(II) electrocatalytic systems in 1.0 M NaOH together with the plot of NCNT/CC in the pure alkaline electrolyte for comparison. The bare NCNT/CC exhibits the highest charge transfer resistance. Addition of glucose, Co(II), and Cu(II) reduces the resistance by 40, 159, and 159 Ω, respectively. When both Co(II) and Cu(II) ions and glucose are introduced, the resistance drops dramatically by 204 Ω. In 1.0 M NaOH, the resistance is

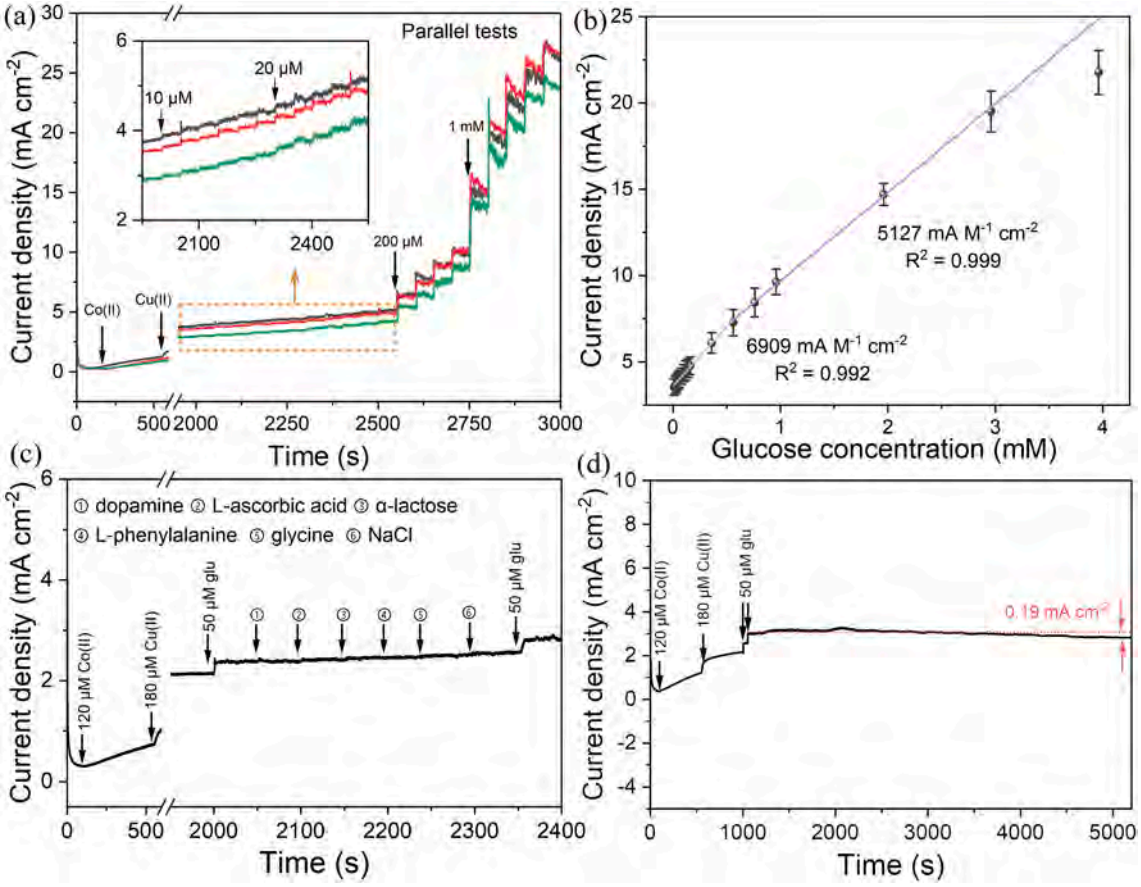

Fig. 5. (a) *i*-t curves and (b) average sensitivity of three NCNT/CC electrodes for glucose detection; (c) Anti-interference and (d) stability in 1.0 M NaOH with Co&Cu at 0.51 V.

determined by the diffusion rate of OH^-. When glucose is added to the electrolyte, the resistance decreases, suggesting that glucose adsorption/desorption is faster than OH^- adsorption/desorption. In the presence of Co(II) or Cu(II), the resistance drops due to Co(II) or Cu(II) oxidation and glucose coordination with Co(II) or Cu(II). In the presence of both glucose and Co(II)&Cu(II), the smallest resistance is observed. It is possible that the coordination between glucose and Co(II)&Cu(II) stabilizes Co(II)&Cu(II) and prevents the formation of oxide and hydroxide for OER.

In order to better understand the electrocatalytic properties of NCNT/CC co-catalyzed by Co(II) and Cu(II), the electrochemical surface area is evaluated based on the double-layer capacitances (C_{dl}) as there is a linear correlation between the two [47]. The C_{dl} values are calculated from the CV curves at different scanning rates (100–200 mV s^{-1}) in the

Table 1
Comparison of the performances for the various types of glucose sensor.

Working electrode	Detection limit (μmol L^{-1})	Linear range (mmol L^{-1})	Sensitivity (mA M^{-1} cm^{-2})	Applied potential(V)	Ref.
Coral-like Cu-Co-O@Ni	0.5	0.0005–1.8	8838.26	+0.60 V (vs. Ag/AgCl)	[33]
$CuCo_2S_4$/CFT	1.01	0.0025–3.67	3852.7	0.35 V (vs. Ag/AgCl)	[48]
$CuCo_2O_4$ NWAs/CC	0.5	0.001–0.93	3930	0.55 V (vs. Ag/AgCl)	[49]
$CuCo_2O_4$/graphite paper	5	0.005–0.32	3625	0.6 V (vs. SCE)	[50]
CuS NCs@Ni_1Co_2 LDHs	0.18	0.001–1.3 mM, 1.3–4.6 mM	2236.4, 920	0.55 V (vs. Ag/AgCl)	[18]
Cu-Co_3O_4	100	0.1–1.0	1613.86	0.6 V	[15]
Cu@Co–MOF	1.6	0.005–0.4, 0.4–1.8	282.89, 113.15	0.6 V (vs. Ag/AgCl)	[51]
CoCu@MC	0.34	0.001–1.25	1489.8	0.65 V (vs. Ag/AgCl)	[52]
Cu-Co NSs	10	0.015–1.21	1171	0.45 V (vs. SCE)	[53]
Cu-CoNSs/CHIT-RGO	10	0.015–6.95	1921	0.45 V (vs. SCE)	[53]
MOF derived CoCu oxides nanorod arrays/CF	0.72	0.001–1.07	11,916	0.5 V (vs. Ag/AgCl)	[54]
Bimetallic NCNT MOF CoCu nanostructure	0.15	0.05–2.5	1027	0.5 V (vs. Ag/AgCl)	[55]
CuCo-600	3	0.005–0.825, 0.005–0.05	567, 1048	0.5 V (vs. SCE)	[56]
PTBA/$CuCo_2O_4$–CNFs	0.15	0.01–0.5, 0.5–1.5	2932, 708		[57]
CC/CuCo oxide-0.12	0.026	0.00005–0.33	4102	0.55 V	[58]
CuCo-P350	2.92	0.005–0.825, 0.1–0.5	1100, 2272	0.55 V (vs. SCE)	[59]
CuCo–CFs	1.0	0.02–11	507	0.6 V (vs. Ag/AgCl)	[60]
NCNT/CC-Co&Cu	0.4	0.0004–0.56, 0.56–2.96	6909, 5127	0.51 V (vs. SCE)	This work

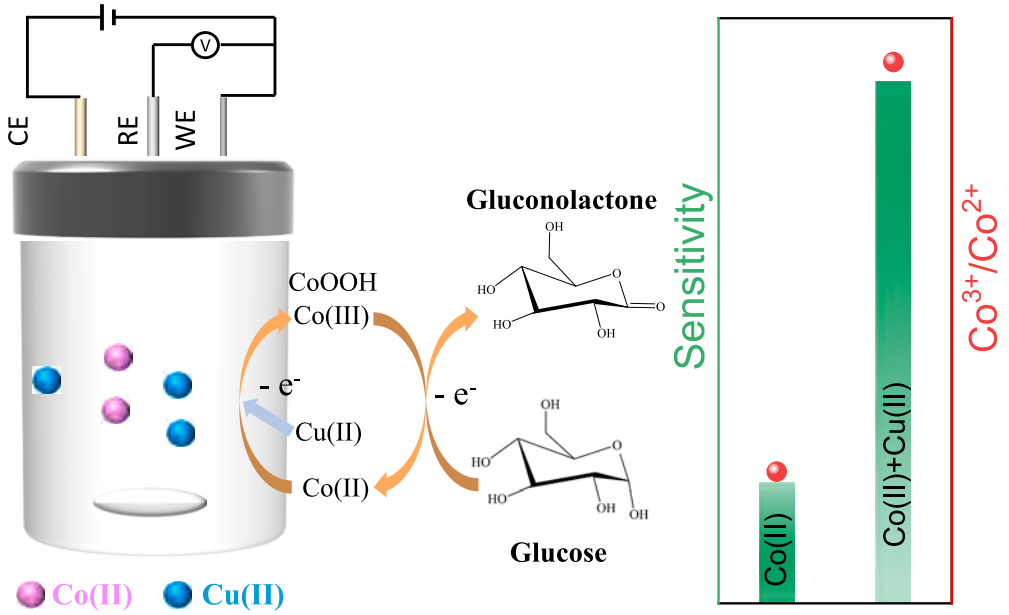

Fig. 6. Mechanism of glucose detection of NCNT/CC co-catalyzed by Co(II) and Cu(II) in the NaOH aqueous solution.

non-Faradaic range (0.2–0.3 V) (Fig. S11). As shown in Fig. 4d, NCNT/CC has a C_{dl} of 3.6 mF cm^{-2} and this value is almost unchanged upon addition of Co(II), Cu(II), and glucose. The results suggest that the metal ions provide the dynamic reaction sites for glucose electrooxidation and the electrode co-catalyzed by bimetallic ions has good stability.

3.6. Reproducibility, selectivity, and stability

The sensitivity, linear range, detection limit, reproducibility, selectivity, and stability are essential criteria to evaluate the electrochemical performance of a sensor. The parameters of the Co(II)&Cu(II) co-catalysis system are evaluated using three NCNT/CC electrodes for glucose detection. The electrochemical catalytic properties of Co&Cu for glucose electrooxidation are evaluated by chronoamperometry. The three parallel *i*-t curves (Fig. 5a) show good reproducibility. The response current of NCNT/CC electrode to glucose co-catalyzed by Co(II)&Cu(II) is linearly correlated with the concentration of glucose with two linear ranges of 0.4 μM – 0.56 mM ($R^2 = 0.992$) and 0.56 mM – 2.96 mM ($R^2 = 0.992$) with a sensitivity of 6,909 and 5,127 mA M^{-1} cm^{-2} (Fig. 5a and 5b), respectively. The relative standard deviation (RSD) (n = 3) is 5.1 % and the LOD (S/N = 3) is calculated to be 0.4 μM. The sensitivity is higher and LOD is lower than most of electrochemical sensors reported previously (Table 1). The electrochemical glucose sensor co-catalyzed by Co(II)&Cu(II) has a low detection limit, quick response, and high sensitivity for glucose determination.

The specificity is another critical parameter. In general, the interference effects show the extent to which the electrode is able to discern glucose from other molecules in the analyte. Interfering species such as dopamine, L-ascorbic acid, α-lactose, L-phenylalanine, glycine, and NaCl often coexist and create challenges to glucose detection. To investigate the selectivity of NCNT/CC co-catalyzed by Co(II)&Cu(II), we carry out interference tests by chronoamperometry in the presence of dopamine, L-ascorbic acid, α-lactose, L-phenylalanine, glycine, and NaCl at 0.51 V in 1.0 M NaOH as shown in Fig. 5c. Upon addition of 50 μM glucose, the current density increases sharply and quickly reaches a stable state, while upon addition of interferences (5 μM), the electrode produces negligible current responses, thus demonstrating that the Co(II)&Cu(II) system has excellent selectivity towards glucose electrooxidation. Moreover, the response currents of spiking glucose before and after introducing interferences are similar, further corroborating that the added interferences do not interfere with glucose detection.

The stability of the system is evaluated by measuring the current response for an extended period in the presence of Co(II) and Cu(II) with 50 μM glucose at 0.51 V. As shown in Fig. 5d, the response current to 50 μM glucose shows a small loss of 0.19 mA cm^{-2} (6.27%) after 4,000 s thus confirming the high stability of the Co(II)&Cu(II) co-catalysis system in the alkaline electrolyte without significant loss of anchored Co(II)&Cu(II) ions.

3.7. Mechanism of co-catalysis by Co(II)&Cu(II)

The glucose electrooxidation mechanism of NCNT/CC co-catalyzed by Co(II)&Cu(II) is presented in Fig. 6. The sensing mechanism stems from the synergistic effects between the Co(II)-glucose complex, CoOOH, and Cu(II) incorporation. Specifically, the mechanism co-catalyzed by Co(II) and Cu(II) in the solution for glucose detection is that Co(II) acts as the dynamic reaction sites and source of the active intermediate (CoOOH), while Cu(II) enhances the formation of CoOOH. The NCNT with a large surface area and good conductivity provides the active sites for Co(II) and Cu(II). Upon glucose addition to the alkaline electrolyte containing Co(II), CoOOH species are generated, while the Co(II)-glucose and Cu(II)-glucose complexes are formed *via* coordination between the d orbitals of the metal and electron donating hydroxy group (OH) of glucose. The complex is a reactant in the double layer region with a finite diffusion behavior. After electron transfer from the complex to the electrode, an intermediate complex evolves featuring high valence metal species coordinated by glucose. Co(II)-glucose undergoes successive electrooxidation of Co(II)-glucose to Co(III)-glucose and Co(IV)-glucose [41]. The Co(IV)-glucose complexes are highly unstable and rearrange to produce Co(III) (or CoOOH) and more stable gluconolactone. Compared the glucose electrooxidation performance catalyzed by bimetallic ions (Co(II) + Co(II)) with that catalyzed by the single metallic ion (Co(II)), obviously improved electroactivity is observed from bimetallic ions catalysis (on the right side of bar graph in Fig. 6). Co(II)-catalysis alone shows more obvious current increase than Cu(II)-catalysis alone (Fig. 2a and 2b), showing that Cu(II) incorporation boosts the formation of CoOOH to improve glucose electrooxidation. Noteworthy, although some active Cu-CoOOH intermediates will *in situ* deposit on the surface of NCNT/CC during the electrochemical process, the Cu-CoOOH modified NCNT/CC exhibits much worse glucose electrooxidation performance in NaOH electrolyte than that NCNT/CC in NaOH + Co(II) + Cu(II) (Fig. S12), indicating that the catalysis effect of

Co(II) + Cu(II) plays the main role in glucose electrooxidation in this system.

The CNT/CC is also used as the working electrode to determine the role of doped N in the NCNT for comparison. The corresponding *i*-t curve is acquired under the same condition as NCNT/CC (Fig. S13). It is evident that NCNT/CC has more stable and higher current increase than CNT/CC, indicating nitrogen provides extra sites for absorption of Co(II) and Cu(II) in NCNT/CC for better glucose detection.

4. Conclusion

A bimetal co-catalytic system is designed for electrochemical detection of glucose by introducing Cu(II)&Cu(II) species into the alkaline solution with NCNT/CC as the working electrode. Co-catalysis by Cu(II)&Cu(II) endows the glucose sensor with excellent reproducibility and sensitivity including a low limit of detection, anti-interference capability, and stability. Systematic materials characterization and electrochemical assessment impart important information about the kinetics and mechanism. Co(II) provides the dynamic reaction sites and source of active intermediate (CoOOH), while Cu(II) enhances the formation of CoOOH. The findings provide insights into bimetal co-catalysis for glucose detection. It indicates that the liquid-phase metal ions catalysis method is promising for the electrochemical sensing for glucose with the property of time- and energy-saving as well as low cost.

CRediT authorship contribution statement

Zanling Huang: Methodology, Investigation, Formal analysis, Writing – original draft. **Shuqi Zhu:** Validation. **Abebe Reda Woldu:** Formal analysis, Writing – review & editing. **Wenhua Gao:** Formal analysis. **Jing-Xin Jian:** Formal analysis. **Paul K. Chu:** Formal analysis, Writing – review & editing. **Qing-Xiao Tong:** Writing – review & editing, Funding acquisition, Supervision. **Liangsheng Hu:** Conceptualization, Writing – review & editing, Funding acquisition, Supervision.

Declaration of Competing Interest

The authors declare that they have no known competing financial interests or personal relationships that could have appeared to influence the work reported in this paper.

Data availability

Data will be made available on request.

Acknowledgements

This work was financially supported by the 2022 Special Fund Project for Science and Technology Innovation Strategy of Guangdong Province (Grant No. STKJ202209077), the Guangdong Province Universities and Colleges Pearl River Scholar Funded Scheme 2019 (GDUPS2019), the 2020 Li Ka Shing Foundation Cross-Disciplinary Research Grant (Grant No. 2020LKSFG01A and 2020LKSFG09A), as well as City University of Hong Kong Donation Research Grant (Grant number DON-RMG No. 9229021).

Appendix A. Supplementary data

Supplementary data to this article can be found online at https://doi.org/10.1016/j.microc.2023.109326.

References

[1] S. Chaiyo, E. Mehmeti, W. Siangproh, T.L. Hoang, H.P. Nguyen, O. Chailapakul, K. Kalcher, Non-enzymatic electrochemical detection of glucose with a disposable paper-based sensor using a cobalt phthalocyanine–ionic liquid–graphene composite, Biosens. Bioelectron. 102 (2018) 113–120, https://doi.org/10.1016/j.bios.2017.11.015.
[2] G. Li, D. Wen, Sensing nanomaterials of wearable glucose sensors, Chinese Chem. Lett. 32 (2021) 221–228, https://doi.org/10.1016/j.cclet.2020.10.028.
[3] B. Zhu, X. Li, L. Zhou, B. Su, An overview of wearable and implantable electrochemical glucose sensors, Electroanal. 34 (2022) 237–245, https://doi.org/10.1002/elan.202100273.
[4] K. Justice Babu, S. Sheet, Y.S. Lee, G. Gnana kumar, Three-dimensional dendrite Cu–Co/reduced graphene oxide architectures on a disposable pencil graphite electrode as an electrochemical sensor for nonenzymatic glucose detection, ACS Sustain, Chem. Eng. 6 (2) (2018) 1909–1918, https://doi.org/10.1021/acssuschemeng.7b03314.
[5] W. Zheng, Y. Li, L. Hu, L.Y.S. Lee, Use of carbon supports with copper ion as a highly sensitive non-enzymatic glucose sensor, Sensor. Actuat. B: Chem. 282 (2019) 187–196, https://doi.org/10.1016/j.snb.2018.10.164.
[6] W. Zheng, Y. Li, L.Y.S. Lee, Bismuth and metal-doped bismuth nanoparticles produced by laser ablation for electrochemical glucose sensing, Sensor. Actuat. B: Chem. 357 (2022), 131334, https://doi.org/10.1016/j.snb.2021.131334.
[7] A.J. Bandodkar, S. Imani, R. Nunez-Flores, R. Kumar, C. Wang, A.M.V. Mohan, J. Wang, P.P. Mercier, Re-usable electrochemical glucose sensors integrated into a smartphone platform, Biosens. Bioelectron. 101 (2018) 181–187, https://doi.org/10.1016/j.bios.2017.10.019.
[8] Y. Xue, A.S. Thalmayer, S. Zeising, G. Fischer, M. Lübke, Commercial and Scientific Solutions for Blood Glucose Monitoring—A Review, Sensors 22 (2022) 425, https://doi.org/10.3390/s22020425.
[9] C. Lin, Y. Du, S. Wang, L. Wang, Y. Song, Glucose oxidase@Cu-hemin metal-organic framework for colorimetric analysis of glucose, Mater. Sci. Eng. C 118 (2021), 111511, https://doi.org/10.1016/j.msec.2020.111511.
[10] L. Chen, E. Hwang, J. Zhang, Fluorescent nanobiosensors for sensing glucose, Sensors 18 (2018) 1440, https://doi.org/10.3390/s18051440.
[11] S. Singh, B.D. Gupta, Fabrication and characterization of a surface plasmon resonance based fiber optic sensor using gel entrapment technique for the detection of low glucose concentration, Sensor. Actuat. B: Chem. 177 (2013) 589–595, https://doi.org/10.1016/j.snb.2012.11.094.
[12] M. Pohanka, Glucose electrochemical biosensors: The past and current trends, Int. J. Electrochem. Sci. 44 (2021) 47, https://doi.org/10.20964/2021.07.52.
[13] X. Sun, Glucose detection through surface-enhanced Raman spectroscopy: a review, Anal. Chim. Acta 1206 (2021), 339226, https://doi.org/10.1016/j.aca.2021.339226.
[14] L. Monti, S. Negri, A. Meucci, A. Stroppa, A. Galli, G. Contarini, Lactose, galactose and glucose determination in naturally "lactose free" hard cheese: HPAEC-PAD method validation, Food Chem. 220 (2017) 18–24, https://doi.org/10.1016/j.foodchem.2016.09.185.
[15] J. Pang, K. Sun, S. Jin, J. Hou, G. Wang, K. Sun, Y. Zheng, Y. Zhang, L. Chen, Oxygen vacancies enriched multi-channel-like metal-doped Co_3O_4 nanosheets by Lewis acid etching for detection of small biological molecules in apple juice and wine, Chem. Eng. J. 454 (2023), 140085, https://doi.org/10.1016/j.cej.2022.140085.
[16] F. Xu, K. Hu, S. Wang, X. Chen, R. Xu, X. Xiong, X. Yuan, M. Zhang, K. Huang, ZIF-8 derived Ni(OH)2 hollow nanocages for non-enzymatic glucose electrochemical sensing, J. Mater. Sci. 57 (2022) 18589–18600, https://doi.org/10.1007/s10853-022-07771-y.
[17] T. Liu, M. Li, P. Dong, Y. Zhang, L. Guo, Design and facile synthesis of mesoporous cobalt nitride nanosheets modified by pyrolytic carbon for the nonenzymatic glucose detection, Sensor. Actuat. B: Chem. 255 (2018) 1983–1994, https://doi.org/10.1016/j.snb.2017.08.218.
[18] T. Yang, W. Zhang, J. Wu, S. Liu, Y. Zhao, Core-shell composite of CuS nanocages and NiCo layered double hydroxide nanosheets with modulated electron structure as "two birds with one Stone" glucose oxidation electrocatalysts, Appl. Surf. Sci. 600 (2022), 154205, https://doi.org/10.1016/j.apsusc.2022.154205.
[19] K. Arikan, H. Burhan, E. Sahin, F. Sen, A sensitive, fast, selective, and reusable enzyme-free glucose sensor based on monodisperse AuNi alloy nanoparticles on activated carbon support, Chemosphere 291 (2022), 132718, https://doi.org/10.1016/j.chemosphere.2021.132718.
[20] B.-D. Hong, K.-L. Hunag, H.-R. Chen, C.-L. Lee, Effect of defective graphene flake for catalysts of supported Pd nanocubes toward glucose oxidation reaction in alkaline medium, J. Electrochem. Soc. 163 (2016) H731, https://doi.org/10.1149/2.0141609jes.
[21] Y. Wang, J. Chen, C. Zhou, L. Zhou, Y. Kong, H. Long, S. Zhong, A novel self-cleaning, non-enzymatic glucose sensor working under a very low applied potential based on a Pt nanoparticle-decorated TiO_2 nanotube array electrode, Electrochim. Acta 115 (2014) 269–276, https://doi.org/10.1016/j.electacta.2013.09.173.
[22] K. Ramachandran, T. Raj kumar, K.J. Babu, G. Gnana kumar, Ni-Co bimetal nanowires filled multiwalled carbon nanotubes for the highly sensitive and selective non-enzymatic glucose sensor applications, Sci. Rep. 6 (1) (2016), https://doi.org/10.1038/srep36583.
[23] A.A. Ensafi, M.M. Abarghoui, B. Rezaei, A new non-enzymatic glucose sensor based on copper/porous silicon nanocomposite, Electrochim. Acta 123 (2014) 219–226, https://doi.org/10.1016/j.electacta.2014.01.031.
[24] X. Niu, M. Lan, H. Zhao, C. Chen, Highly sensitive and selective nonenzymatic detection of glucose using three-dimensional porous nickel nanostructures, Anal. Chem. 85 (2013) 3561–3569, https://doi.org/10.1021/ac3030976.
[25] M.d. Asaduzzaman, M.A. Zahed, M.d. Sharifuzzaman, M.S. Reza, X. Hui, S. Sharma, Y.D. Shin, J.Y. Park, A hybridized nano-porous carbon reinforced 3D graphene-based epidermal patch for precise sweat glucose and lactate analysis, Biosens. Bioelectron. 219 (2023) 114846.

[26] E. Sehit, Z. Altintas, Significance of nanomaterials in electrochemical glucose sensors: An updated review (2016–2020), Biosens. Bioelectron. 159 (2020), 112165, https://doi.org/10.1016/j.bios.2020.112165.
[27] M. Li, C. Han, Y. Zhang, X. Bo, L. Guo, Facile synthesis of ultrafine Co_3O_4 nanocrystals embedded carbon matrices with specific skeletal structures as efficient non-enzymatic glucose sensors, Anal. Chim. Acta 861 (2015) 25–35, https://doi.org/10.1016/j.aca.2014.12.030.
[28] Y. Mu, D. Jia, Y. He, Y. Miao, H.-L. Wu, Nano nickel oxide modified non-enzymatic glucose sensors with enhanced sensitivity through an electrochemical process strategy at high potential, Biosens. Bioelectron. 26 (2011) 2948–2952, https://doi.org/10.1016/j.bios.2010.11.042.
[29] P. Subramanian, J. Niedziolka-Jonsson, A. Lesniewski, Q. Wang, M. Li, R. Boukherroub, S. Szunerits, Preparation of reduced graphene oxide–Ni(OH)2 composites by electrophoretic deposition: application for non-enzymatic glucose sensing, J. Mater. Chem. A 2 (2014) 5525–5533, https://doi.org/10.1039/C4TA00123K.
[30] Q. Dong, H. Ryu, Y. Lei, Metal oxide based non-enzymatic electrochemical sensors for glucose detection, Electrochim. Acta 370 (2021), 137744, https://doi.org/10.1016/j.electacta.2021.137744.
[31] G.A. Naikoo, H. Salim, I.U. Hassan, T. Awan, F. Arshad, M.Z. Pedram, W. Ahmed, A. Qurashi, Recent Advances in Non-Enzymatic Glucose Sensors Based on Metal and Metal Oxide Nanostructures for Diabetes Management-A Review, Front. Chem. (2021) 786, https://doi.org/10.3389/fchem.2021.748957.
[32] D.-W. Hwang, S. Lee, M. Seo, T.D. Chung, Recent advances in electrochemical non-enzymatic glucose sensors–a review, Anal. Chim. Acta (2018) 1–34, https://doi.org/10.1016/j.aca.2018.05.051.
[33] R.-M. Yuan, H.-J. Li, X.-M. Yin, H.-Q. Wang, J.-H. Lu, L.-L. Zhang, Coral-like Cu-Co-mixed oxide for stable electro-properties of glucose determination, Electrochim. Acta 273 (2018) 502–510, https://doi.org/10.1016/j.electacta.2018.04.003.
[34] Z.-Z. Ma, Y.-S. Wang, B. Liu, H. Jiao, L. Xu, A Non-Enzymatic Electrochemical Sensor of Cu@ Co–MOF Composite for Glucose Detection with High Sensitivity and Selectivity, Chemosensors 10 (2022) 416, https://doi.org/10.3390/chemosensors10100416.
[35] X. Duan, K. Liu, Y. Xu, M. Yuan, T. Gao, J. Wang, Nonenzymatic electrochemical glucose biosensor constructed by $NiCo_2O_4$@ Ppy nanowires on nickel foam substrate, Sensor. Actuat. B: Chem. 292 (2019) 121–128, https://doi.org/10.1016/j.snb.2019.04.107.
[36] S. Song, X. Ma, W. Li, B. Zhang, B. Shao, X. Chang, X. Liu, Novel stylophora coral-like furan-based Ni/Co bimetallic metal organic framework for high-performance capacitive storage and non-enzymatic glucose electrochemical sensing, J. Alloy. Compd. 931 (2023), 167413, https://doi.org/10.1016/j.jallcom.2022.167413.
[37] S. Bilal, W. Ullah, Polyaniline@CuNi nanocomposite: A highly selective, stable and efficient electrode material for binder free non-enzymatic glucose sensor, Electrochim. Acta 284 (2018) 382–391, https://doi.org/10.1016/j.electacta.2018.07.165.
[38] M. Tan, M. Ni, X. Liu, B. Qu, X. Lin, D. Jiang, Y. Yuan, H. Du, Surface adsorption guided design of semicrystalline nickel-iron hydroxide for highly-sensitive glucose sensing, Chem. Eng. J. 451 (2023), 138963, https://doi.org/10.1016/j.cej.2022.138963.
[39] Z. Wang, J. Zhang, R. Jian, J. Liao, X. Xiong, K. Huang, Room temperature ultrafast synthesis of zinc oxide nanomaterials via hydride generation for non-enzymatic glucose detection, Microchem. J. 159 (2020) 105396, https://doi.org/10.1016/j.microc.2020.105396.
[40] Z. Wang, J. Zhang, Q. Yu, H. Yang, X. Chen, X. Yuan, K. Huang, X. Xiong, Synthesis of 3D CoO nanowires supported NiFe layered double hydroxide using an atmospheric pressure microplasma for high-performance oxygen evolution reaction, Chem. Eng. J. 410 (2021) 128366, https://doi.org/10.1016/j.cej.2020.128366.
[41] W. Zheng, Y. Li, L.Y.S. Lee, Insights into the transition metal ion-mediated electrooxidation of glucose in alkaline electrolyte, Electrochim. Acta 308 (2019) 9–19, https://doi.org/10.1016/j.electacta.2019.04.007.
[42] W. Zheng, Y. Li, C.S. Tsang, L. Hu, M. Liu, B. Huang, L.Y.S. Lee, K.Y. Wong, CuII-Mediated Ultra-efficient Electrooxidation of Glucose, ChemElectroChem 4 (2017) 2788–2792, https://doi.org/10.1002/celc.201700712.
[43] G. Xie, G. Li, D. Chen, X. Meng, C. Fan, B. Pang, Y. Zhang, Y. Chen, L. Yu, L. Dong, Highly sensitive non-enzymatic glucose sensor based on CoCu@ MC derived from CoCu/melamine cyanurate superstructures, Diam. Relat. Mater. 130 (2022), 109509, https://doi.org/10.1016/j.diamond.2022.109509.
[44] W. Zheng, Y. Li, M. Liu, C.S. Tsang, L.Y.S. Lee, K.Y. Wong, Cu2+-doped Carbon Nitride/MWCNT as an Electrochemical Glucose Sensor, Electroanal. 30 (2018) 1446–1454, https://doi.org/10.1002/elan.201800076.
[45] S. Liu, S. Dou, J. Meng, Y. Liu, Y. Liu, H. Yu, Efficient biobased carboxylic acids synthesis by synergistic electrocatalysis of multi-active sites on bimetallic Cu-Co oxide/oxyhydroxide, Appl. Catal. B: Environ. 331 (2023), 122709, https://doi.org/10.1016/j.apcatb.2023.122709.
[46] L. Yan, B. Zhang, Z. Liu, J. Zhu, Synergy of copper doping and oxygen vacancies in porous CoOOH nanoplates for efficient water oxidation, Chem. Eng. J. 405 (2021), 126198, https://doi.org/10.1016/j.cej.2020.126198.
[47] J. Zhang, S. Geng, R. Li, X. Zhang, Y. Zhou, T. Yu, Y. Wang, S. Song, Z. Shao, Novel monoclinic ABO_4 oxide with single-crystal structure as next generation electrocatalyst for oxygen evolution reaction, Chem. Eng. J. 420 (2021), 130492, https://doi.org/10.1016/j.cej.2021.130492.
[48] W. Xu, J. Lu, W. Huo, J. Li, X. Wang, C. Zhang, X. Gu, C. Hu, Direct growth of $CuCo_2S_4$ nanosheets on carbon fiber textile with enhanced electrochemical pseudocapacitive properties and electrocatalytic properties towards glucose oxidation, Nanoscale 10 (2018) 14304–14313, https://doi.org/10.1039/C8NR04519D.
[49] X. Luo, M. Huang, L. Bie, D. He, Y. Zhang, P. Jiang, $CuCo_2O_4$ nanowire arrays supported on carbon cloth as an efficient 3D binder-free electrode for non-enzymatic glucose sensing, RSC Adv. 7 (2017) 23093–23101, https://doi.org/10.1039/C7RA01840A.
[50] S. Liu, K.S. Hui, K.N. Hui, Flower-like copper cobaltite nanosheets on graphite paper as high-performance supercapacitor electrodes and enzymeless glucose sensors, ACS Appl. Mater. Interfaces 8 (2016) 3258–3267, https://doi.org/10.1021/acsami.5b11001.
[51] Z.-Z. Ma, Y.-S. Wang, B. Liu, H. Jiao, L. Xu, A Non-Enzymatic Electrochemical Sensor of Cu@Co–MOF Composite for Glucose Detection with High Sensitivity and Selectivity, Chemosensors 10 (2022) 416, https://doi.org/10.3390/chemosensors10100416.
[52] G. Xie, G. Li, D. Chen, X. Meng, C. Fan, B. Pang, Y. Zhang, Y. Chen, L. Yu, L. Dong, Highly sensitive non-enzymatic glucose sensor based on CoCu@MC derived from CoCu/melamine cyanurate superstructures, Diam. Relat. Mater. 130 (2022), 109509, https://doi.org/10.1016/j.diamond.2022.109509.
[53] L. Wang, Y. Zheng, X. Lu, Z. Li, L. Sun, Y. Song, Dendritic copper-cobalt nanostructures/reduced graphene oxide-chitosan modified glassy carbon electrode for glucose sensing, Sensor. Actuat. B-Chem. 195 (2014) 1–7, https://doi.org/10.1016/j.snb.2014.01.007.
[54] C. Wei, X. Li, W. Xiang, Z. Yu, Q. Liu, MOF derived seaweed-like CoCu oxides nanorod arrays for electrochemical non-enzymatic glucose sensing with ultrahigh sensitivity, Sensor. Actuat. B-Chem. 324 (2020), 128773, https://doi.org/10.1016/j.snb.2020.128773.
[55] S.E. Kim, A. Muthurasu, Highly Oriented Nitrogen-doped Carbon Nanotube Integrated Bimetallic Cobalt Copper Organic Framework for Non-enzymatic Electrochemical Glucose and Hydrogen Peroxide Sensor, Electroanal. 33 (2021) 1333–1345, https://doi.org/10.1002/elan.202060566.
[56] G. Ni, F. Wang, Z. Pan, R. Zhang, Bimetallic CuCo derived from Prussian blue analogue for nonenzymatic glucose sensing, Electroanal. 33 (2021) 845–853, https://doi.org/10.1002/elan.202060402.
[57] Y. Ding, H. Sun, C. Ren, M. Zhang, K. Sun, A nonenzymatic glucose sensor platform based on specific recognition and conductive polymer-decorated $CuCo_2O_4$ carbon nanofibers, Materials 13 (2020) 2874, https://doi.org/10.3390/ma13122874.
[58] L. Long, X. Liu, L. Chen, S. Wang, M. Liu, J. Jia, MOF-derived 3D leaf-like CuCo oxide arrays as an efficient catalyst for highly sensitive glucose detection, Electrochim. Acta 308 (2019) 243–252, https://doi.org/10.1016/j.electacta.2019.04.039.
[59] F. Cao, Y. Zhou, J. Wu, W. Li, C. Zhang, G. Ni, P. Cui, C. Song, Electrospinning one-dimensional surface-phosphorized CuCo/C nanofibers for enzyme-free glucose sensing, New J. Chem. 46 (2022) 11531–11539, https://doi.org/10.1039/D2NJ01485H.
[60] M. Li, L. Liu, Y. Xiong, X. Liu, A. Nsabimana, X. Bo, L. Guo, Bimetallic MCo (M= Cu, Fe, Ni, and Mn) nanoparticles doped-carbon nanofibers synthetized by electrospinning for nonenzymatic glucose detection, Sensor. Actuat. B-Chem. 207 (2015) 614–622, https://doi.org/10.1016/j.snb.2014.10.092.

Supporting Information

Outstanding glucose sensing properties of N-doped carbon nanotubes boosted by Co(II) and Cu(II) ions in alkaline electrolytes

Zanling Huang[a], Shuqi Zhu[a], Abebe Reda Woldu[a], Wenhua Gao[a], Jing-Xin Jian[a], Paul K. Chu[c], Qing-Xiao Tong[a,*], and Liangsheng Hu[a,b,*]

[a] Department of Chemistry and Key Laboratory for Preparation and Application of Ordered Structural Materials of Guangdong Province, Shantou University, Shantou, 515063, P. R. China

[b] Chemistry and Chemical Engineering Guangdong Laboratory, Shantou, 515063, P. R. China

[c] Department of Physics, Department of Materials Science and Engineering, and Department of Biomedical Engineering, City University of Hong Kong, Tat Chee Avenue, Kowloon, Hong Kong, China

ORCID: 0000-0002-5581-4883 (P.K. Chu); 0000-0002-4133-2090 (L.S. Hu)

* Correspondence: qxtong@stu.edu.cn (Q.X. Tong), lshu@stu.edu.cn (L. S. Hu)

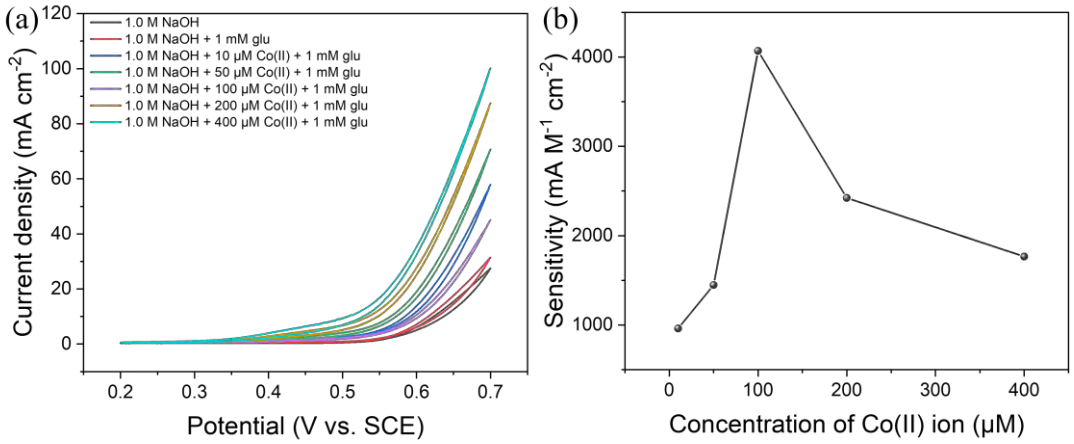

Fig. S1. (a) CVs of NCNT/CC in 1.0 M NaOH, 1.0 M NaOH with 1 mM glucose, and 1.0 M NaOH with 1 mM glucose and different concentrations (10, 50, 100, 200, 400 μM) of Co(II); (b) Sensitivity of NCNT/CC in 1.0 M NaOH with different concentrations (10, 50, 100, 200, 400 μM) of Co(II) at 0.51 V.

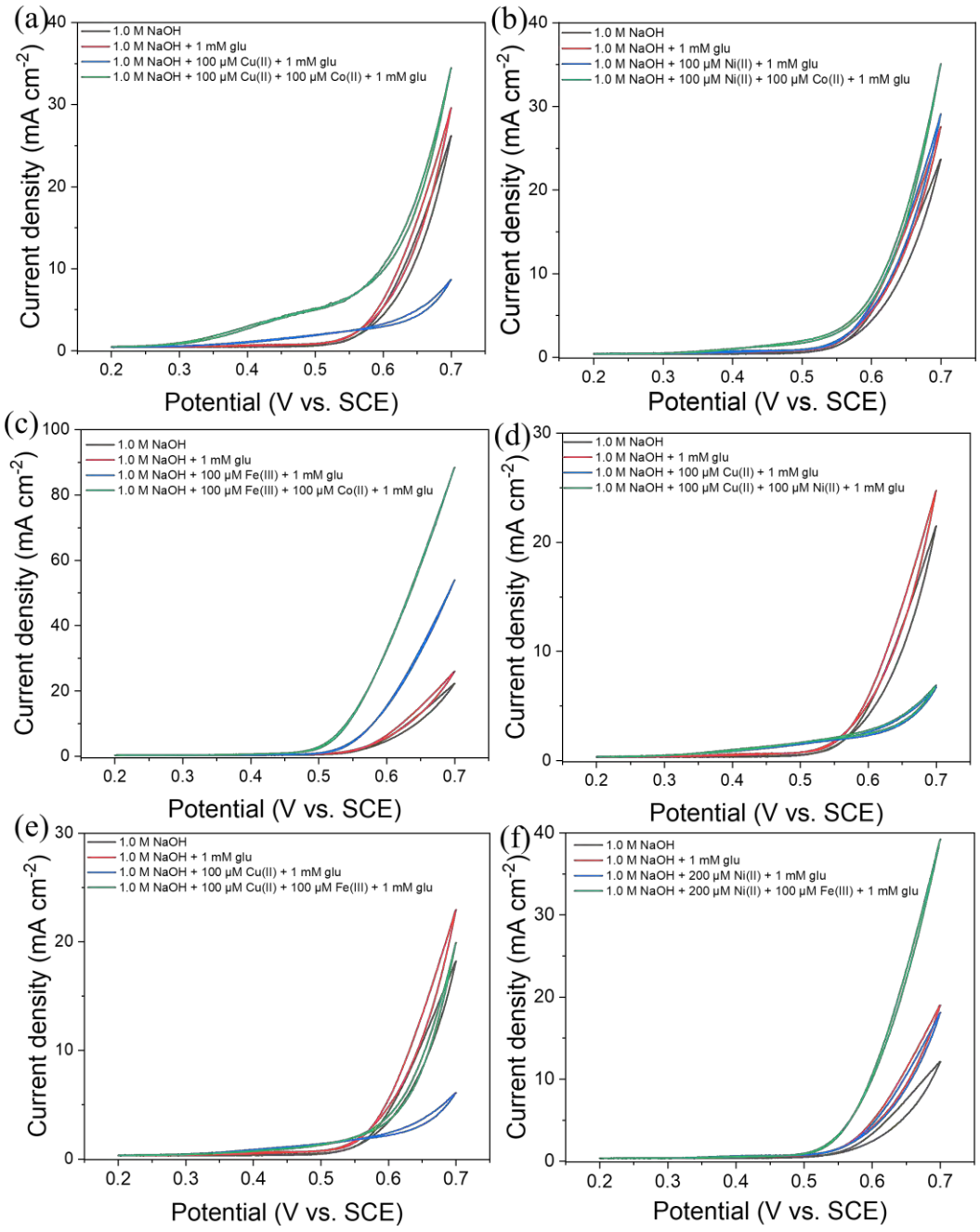

Fig. S2. CVs of NCNT/CC in 1.0 M NaOH, 1.0 M NaOH with 1 mM glucose, 1.0 M NaOH with 1 mM glucose, and different combinations of bimetal-ions including (a) Cu(II) and Co(II), (b) Ni(II) and Cu(II), (c) Fe(III) and Co(II), (d) Cu(II) and Ni(II), (e) Cu(II) and Fe(III), and (f) Ni(II) and Fe(III).

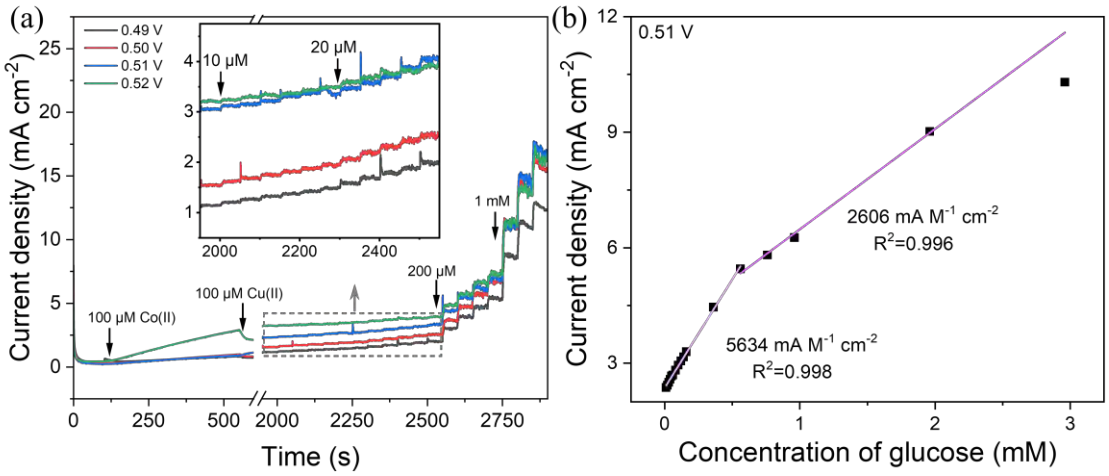

Fig. S3. *i*-t curves of NCNT/CC in 1.0 M NaOH with 100 μM Co(II) + 100 μM Cu(II) at different applied potentials (0.49, 0.50, 0.51, and 0.52 V). (b) Sensitivity of NCNT/CC in 1.0 M NaOH with 100 μM Co(II) + 100 μM Cu(II) at 0.51 V.

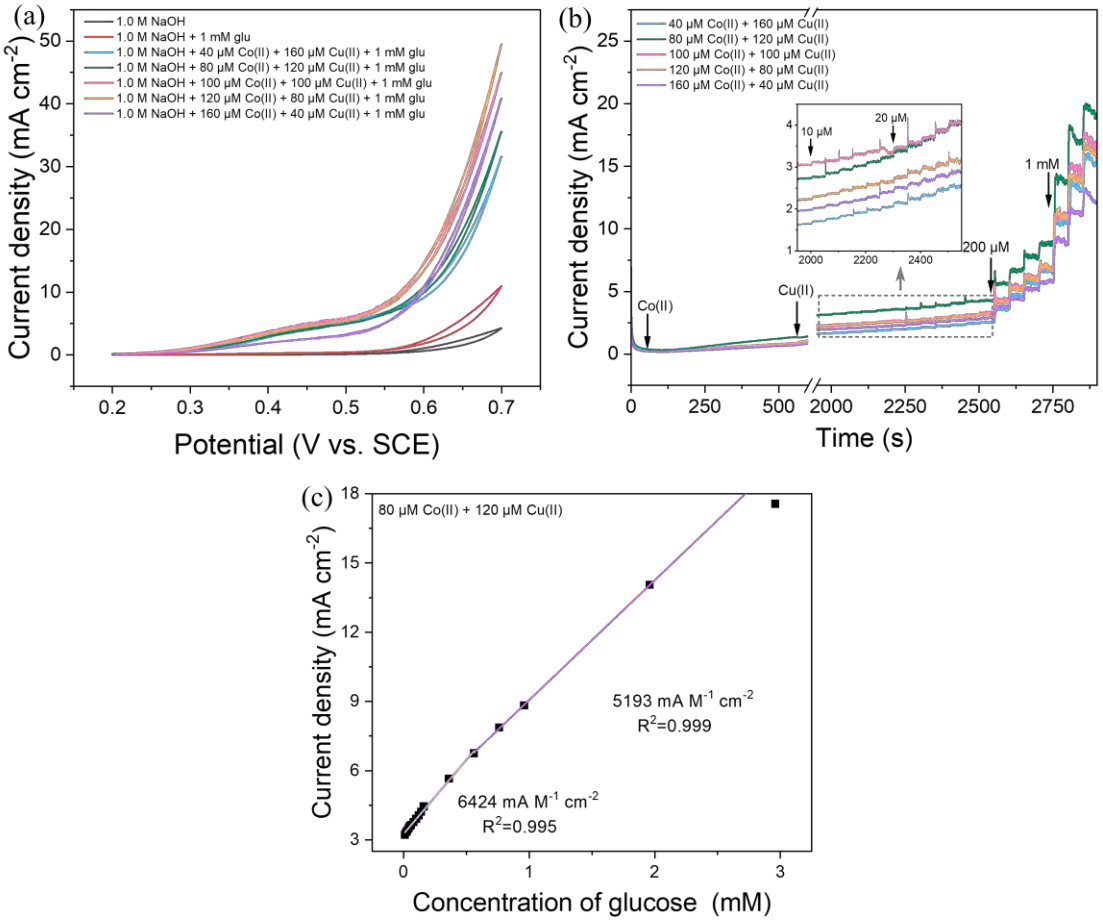

Fig. S4. (a) CVs of NCNT/CC in 1.0 M NaOH, 1.0 M NaOH with 1 mM glucose, and 1.0 M NaOH with 1 mM glucose and different ions concentration ratios (c(Co(II):c(Cu(II) = 1:4, 2:3, 1:1, 3:2, and 4:1, total ions concentration of 200 μM) at 0.51 V; (b) *i*-t curves of NCNT/CC in 1.0 NaOH with different ion concentration ratios (c(Co(II):c(Cu(II) = 1:4, 2:3, 1:1, 3:2, and 4:1, total ion concentration of 200 μM) at 0.51 V; (c) Sensitivity of NCNT/CC in 1.0 NaOH with 80 μM Co(II) + 120 μM Cu(II) at 0.51 V.

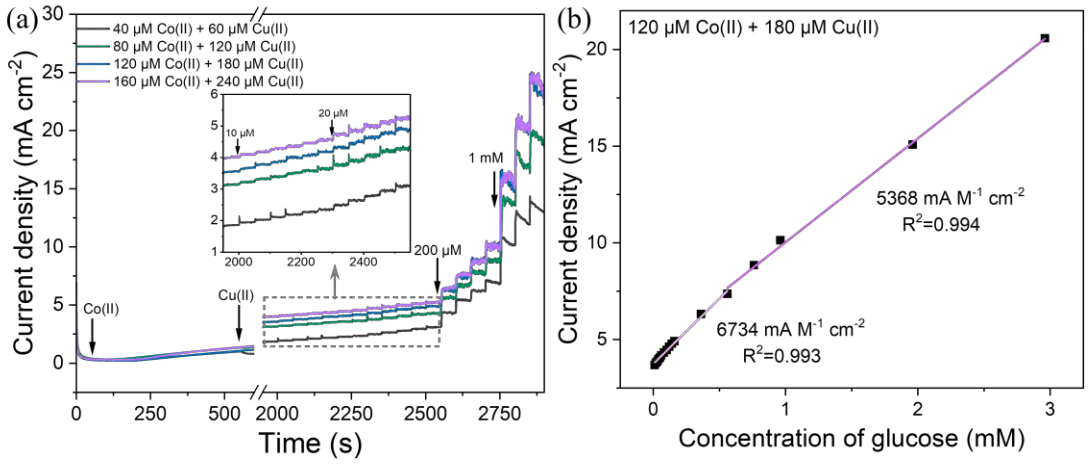

Fig. S5. (a) *i*-t curves of NCNT/CC in 1.0 M NaOH with different total ion concentrations (100, 200, 300, and 400 μM, c(Co(II):c(Cu(II) = 2:3) at 0.51 V and (b) Sensitivity of NCNT/CC in 1.0 NaOH with 120 μM Co(II) + 180 μM Cu(II) at 0.51 V.

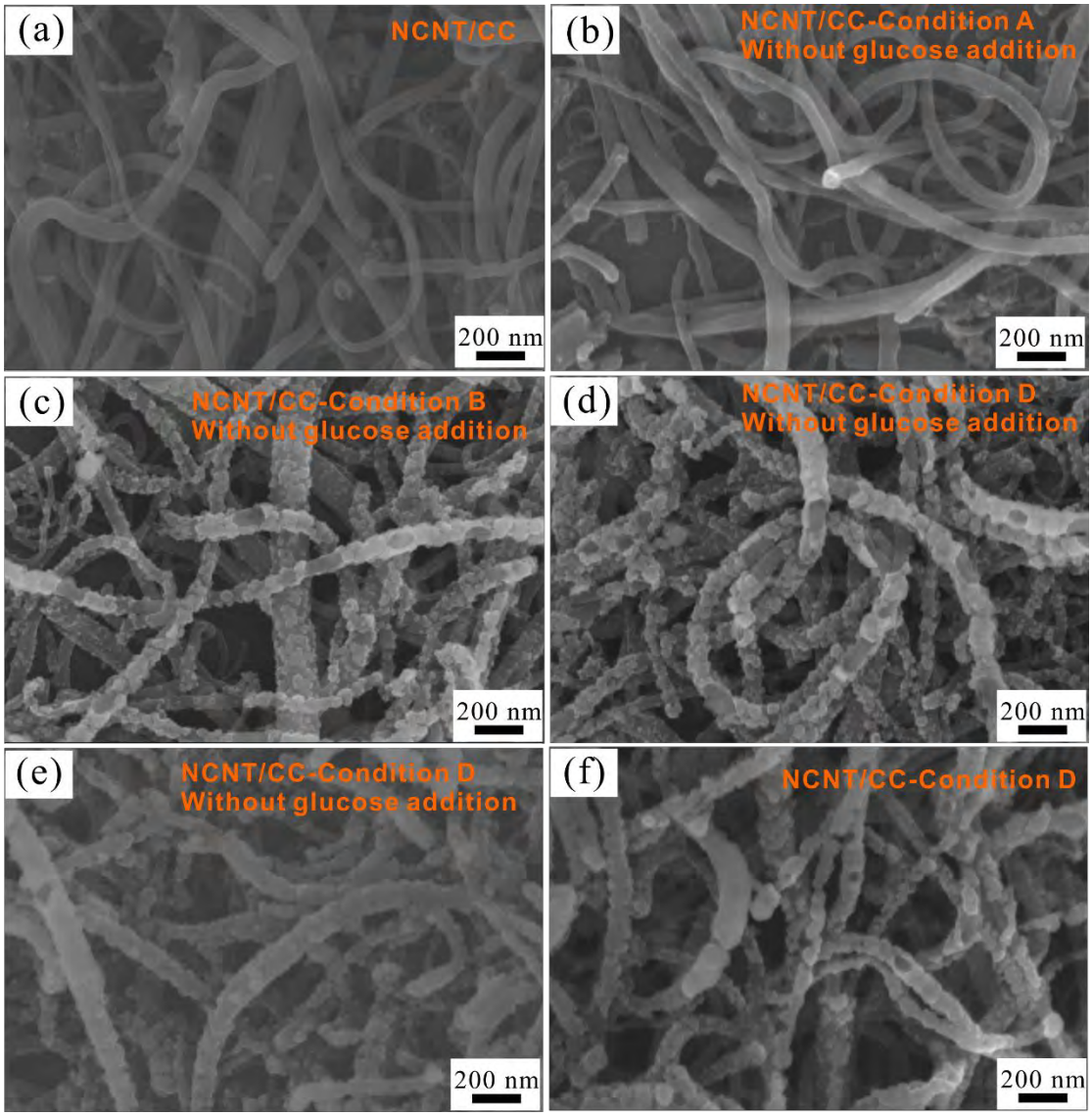

Fig. S6. SEM images of (a) Blank NCNT/CC, (b)-(f) NCNT/CC after testing under different conditions; (b) Condition A: *i*-t test in 1.0 M NaOH with 180 μM Cu(II) at 0.51 V for 1000 s (before glucose addition); (c) Condition B: *i*-t test in 1.0 M NaOH with 120 μM Co(II) at 0.51 V for 1,000 s (before glucose addition); (d) Condition D: *i*-t test in 1.0 M NaOH with 120 μM Co(II) + 180 μM Cu(II) at 0.51 V for 1000 s (before glucose addition); (e) Condition D: *i*-t test in 1.0 M NaOH with 120 μM Co(II) + 180 μM Cu(II) at 0.51 V for 2,200 s (the same time as glucose detection); (f) Condition D: glucose detection catalyzed by 120 μM Co(II) + 180 μM Cu(II).

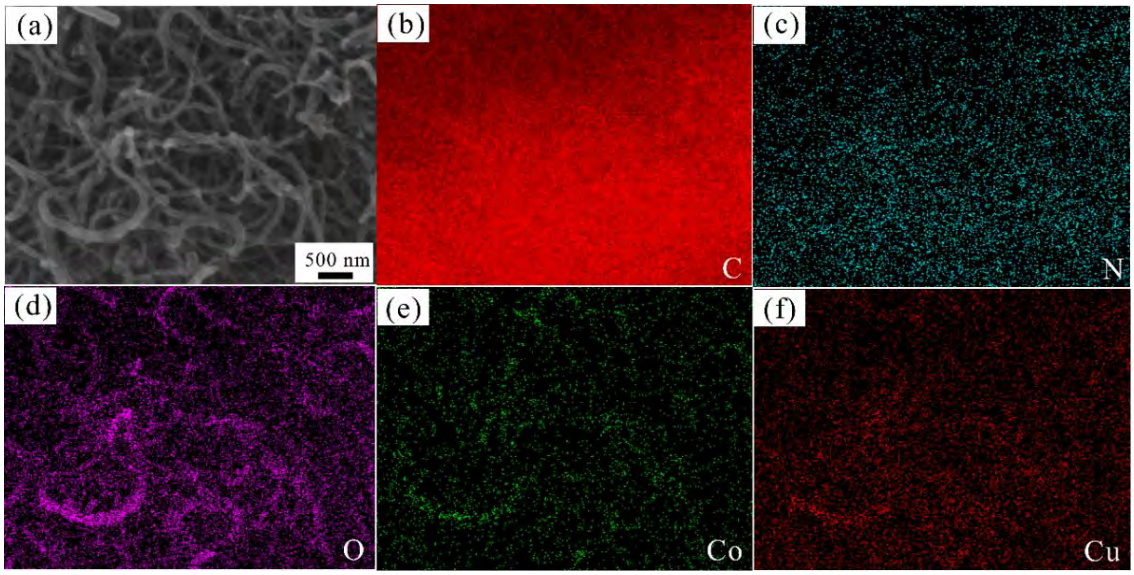

Fig. S7. EDS elemental maps of NCNT/CC after glucose detection.

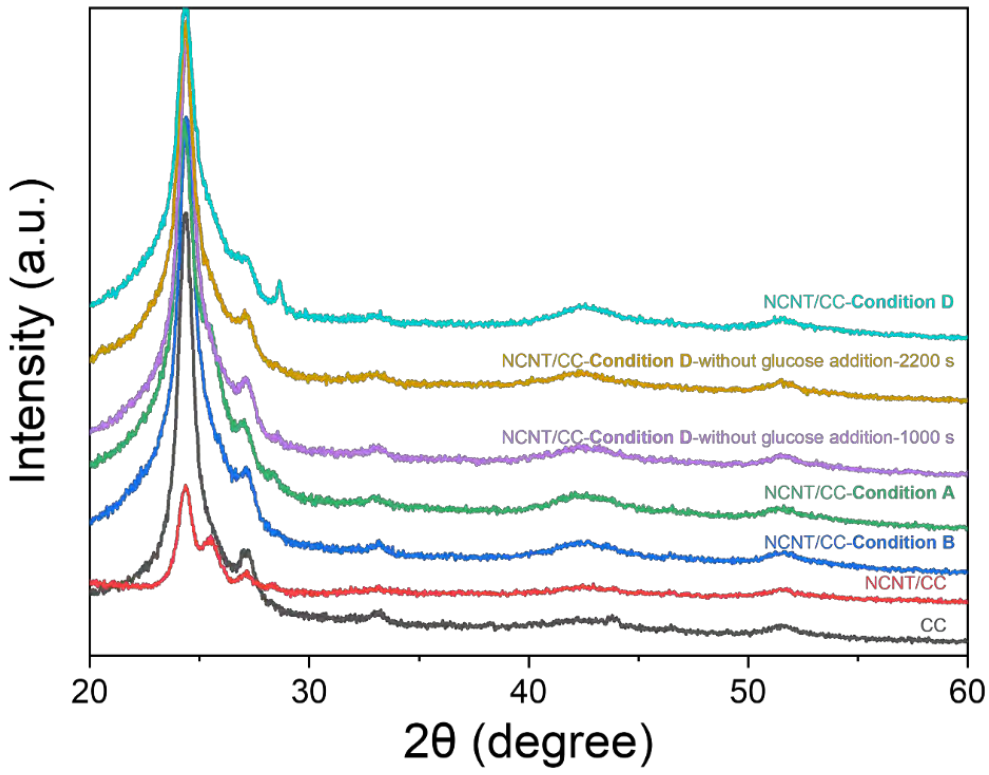

Fig. S8. XRD patterns of CC, blank NCNT/CC, NCNT/CC after testing under different conditions. Condition B: *i*-t test in 1.0 M NaOH with 120 μM Co(II) at 0.51 V for 1000 s (before glucose addition); Condition A: *i*-t test in 1.0 M NaOH with 180 μM Cu(II) at 0.51 V for 1000 s (before glucose addition); Condition D: *i*-t test in 1.0 M NaOH with 120 μM Co(II) + 180 μM Cu(II) at 0.51 V for 1000 s (before glucose addition); Condition D: *i*-t test in 1.0 M NaOH with 120 μM Co(II) + 180 μM Cu(II) at 0.51 V for 2200 s (the same time as glucose detection) and glucose detection (Condition D).

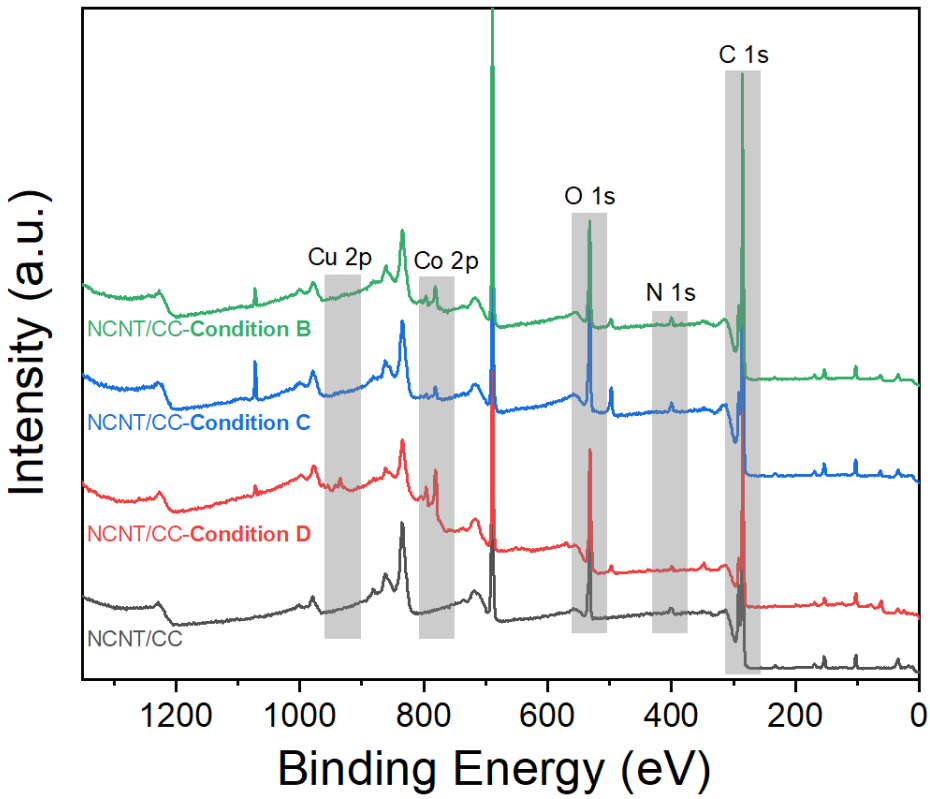

Fig. S9. XPS survey spectra of the blank NCNT/CC electrode and NCNT/CC after glucose detection catalyzed by Co&Cu(II) (Condition D), Cu(II)&Co (Condition C), and Co (Condition B).

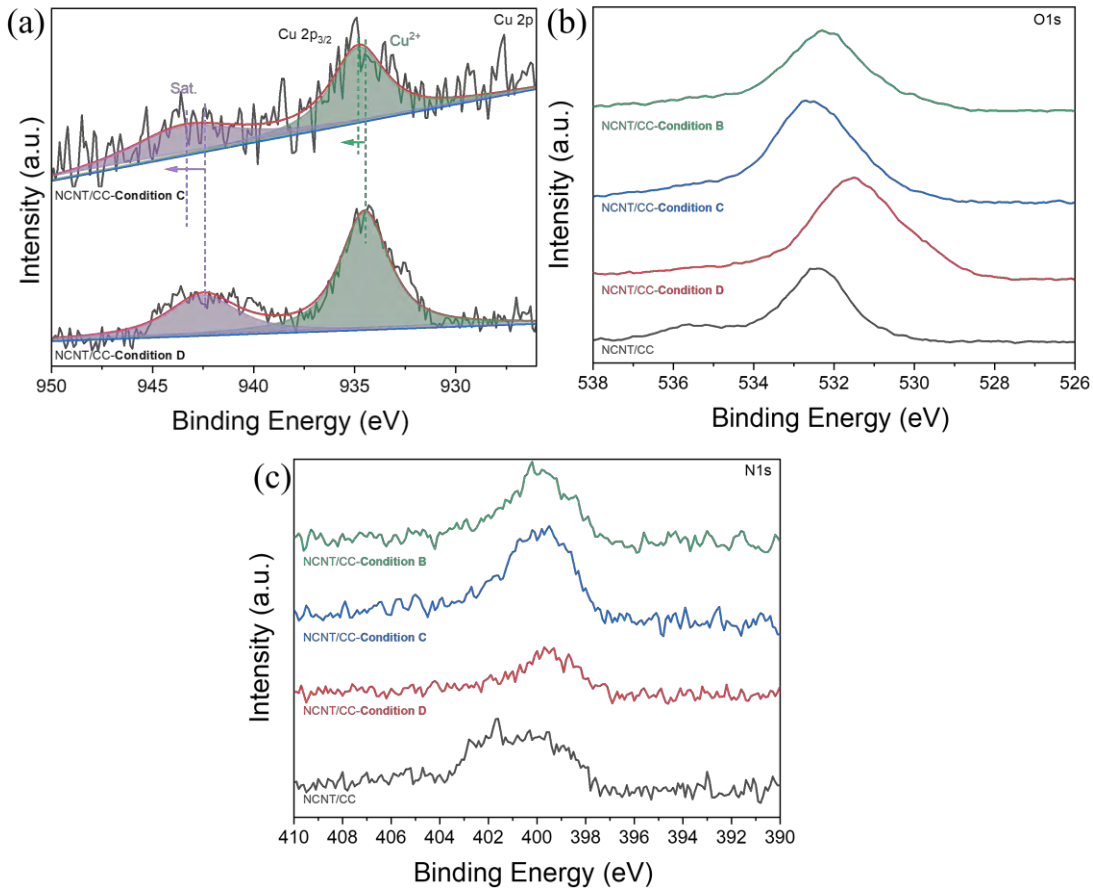

Fig. S10. (a) Cu 2*p* spectra of NCNT/CC catalyzed by Co&Cu and Cu&Co after glucose detection; (b) O 1*s* and (c) N 1*s* spectra of NCNT/CC and NCNT/CC after glucose detection.

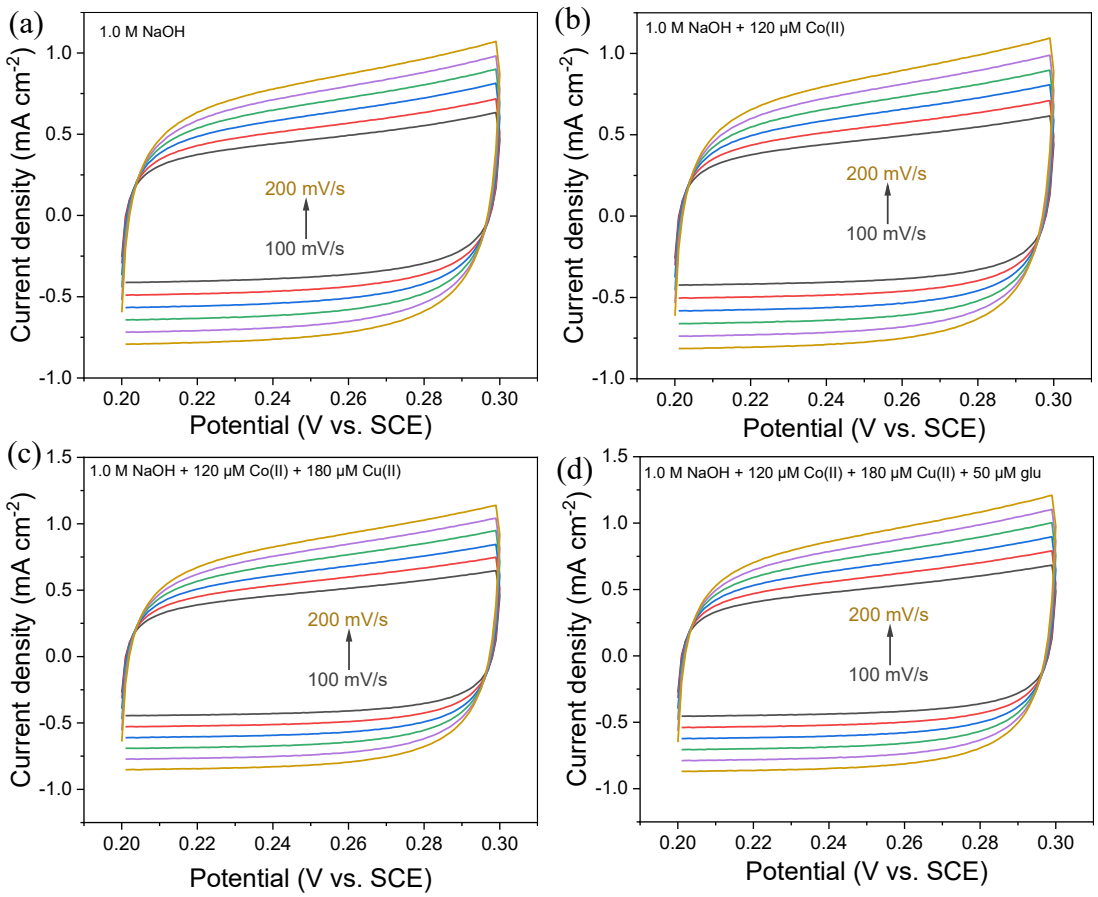

Fig. S11. CVs of NCNT/CC between the range of 0.2-0.3 V at different scanning rates in (a) 1.0 M NaOH, (b) 1.0 M NaOH with 120 μM Co(II), (c) 1.0 NaOH with 120 μM Co(II) + 180 μM Cu(II), and (d) 1.0 NaOH with 120 μM Co(II) + 180 μM Cu(II) and 50 μM glucose.

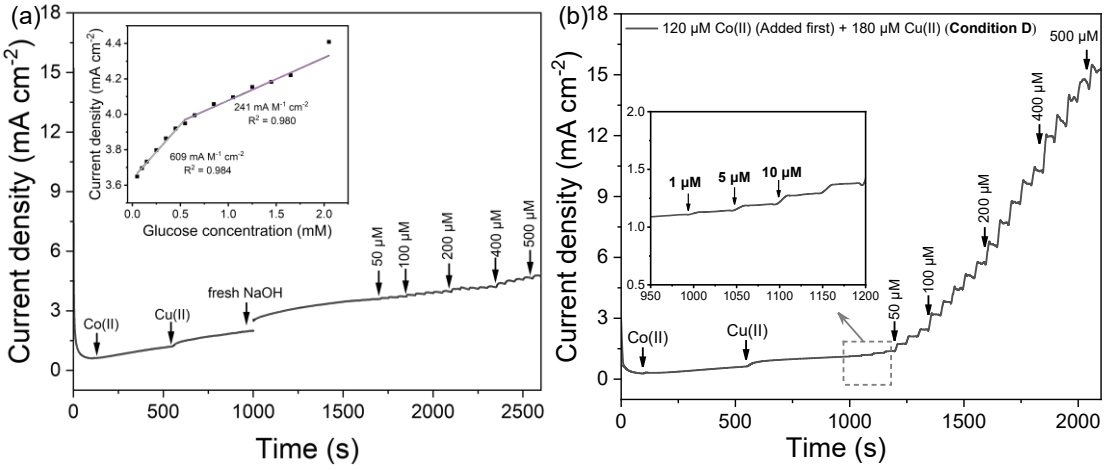

Fig. S12. (a) *i*-t curves of NCNT/CC towards glucose electrooxidation in 1.0 M NaOH at 0.51 V (inset is the sensitivity of glucose detection). Before glucose detection, the electrode was performed with *i*-t test in 1.0 M NaOH with 120 μM Co(II) + 180 μM Cu(II), and then the electrolyte was replaced by fresh 1.0 M NaOH for glucose detection. (b) *i*-t curves of NCNT/CC towards glucose electrooxidation in 1.0 M NaOH with 120 μM Co(II) + 180 μM Cu(II) at 0.51 V.

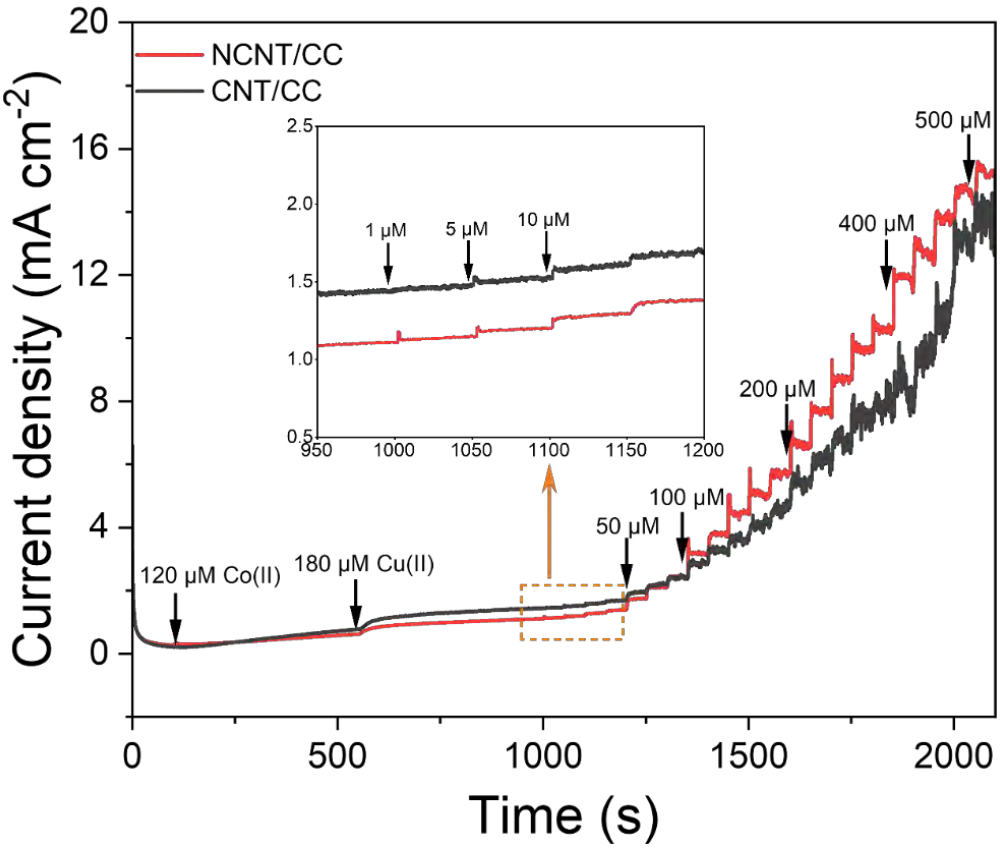

Fig. S13. *i*-t curves of NCNT/CC and CNT/CC in 1.0 M NaOH with 120 μM Co(II) + 180 μM Cu(II) at 0.51 V.